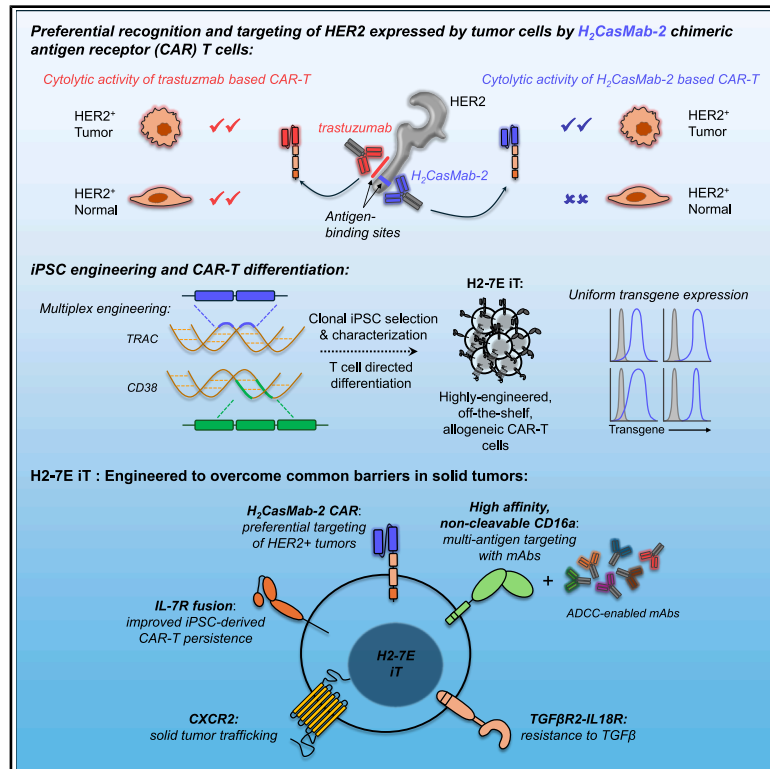


Preferential tumor targeting of HER2 by iPSC-derived CAR T cells engineered to overcome multiple barriers to solid tumor efficacy

Graphical abstract



Authors

Martin P. Hosking, Soheila Shirinbak, Kyla Omilusik, ..., Takao Arimori, Yukinari Kato, Bahram Valamehr

Correspondence

martin.hosking@fatetherapeutics.com (M.P.H.),
bob.valamehr@fatetherapeutics.com (B.V.)

In brief

Hosking and colleagues have generated and preclinically characterized an off-the-shelf, allogeneic CAR T cell, derived from an induced pluripotent stem cell, that is intended to target HER2 on cancer cells without harming HER2-expressing healthy cells. Additional genetic edits have been specifically introduced to improve and sustain activity within solid tumors.

Highlights

- Differential recognition of tumor and normal cells by HER2-directed CAR
- Multiplex editing of iPSC to generate H2-7E cells with uniform transgene expression
- H2-7E mediate multi-antigen tumor targeting via HER2 CAR and hnCD16
- H2-7E demonstrate enhanced persistence, improved trafficking, and TGF-β resistance

Article

Preferential tumor targeting of HER2 by iPSC-derived CAR T cells engineered to overcome multiple barriers to solid tumor efficacy

Martin P. Hosking,^{1,6,*} Soheila Shirinbak,^{1,5} Kyla Omilusik,^{1,5} Shilpi Chandra,^{1,5} Mika K. Kaneko,³ Angela Gentile,¹ Susumu Yamamoto,² Bishwas Shrestha,¹ Joy Grant,¹ Megan Boyett,¹ Demetrio Cardenas,¹ Hannah Keegan,¹ Samad Ibitokou,¹ Carolina Pavon,¹ Takahiro Mizoguchi,² Tatsuya Ihara,² Daisuke Nakayama,² Ramzey Abujarour,¹ Tom T. Lee,¹ Raedun Clarke,¹ Jode Goodridge,¹ Eigen Peralta,¹ Tatsuo Maeda,² Junichi Takagi,⁴ Takao Arimori,⁴ Yukinari Kato,³ and Bahram Valamehr^{1,*}

¹Fate Therapeutics, Inc., San Diego, CA, USA

²Minase Research Institute, Ono Pharmaceutical Co., Ltd., Osaka, Japan

³Department of Antibody Drug Development, Tohoku University Graduate School of Medicine, 2-1 Seiryomachi, Aoba-ku, Sendai 980-8575, Miyagi, Japan

⁴Institute for Protein Research, Osaka University, 3-2, Yamadaoka, Suita 565-0871, Osaka, Japan

⁵These authors contributed equally

⁶Lead contact

*Correspondence: martin.hosking@fatetherapeutics.com (M.P.H.), bob.valamehr@fatetherapeutics.com (B.V.)

<https://doi.org/10.1016/j.stem.2025.05.007>

SUMMARY

Chimeric antigen receptor (CAR) T cell therapies in solid tumors have been limited by on-target, off-tumor toxicity, antigen heterogeneity, and an inability to simultaneously overcome multiple diverse resistance mechanisms within the tumor microenvironment that attenuate anti-tumor activity. Here, we describe an induced pluripotent stem cell (iPSC)-derived CAR T cell that combines a human epidermal growth factor receptor 2 (HER2)-targeting CAR—differentially recognizing tumor from normal cells and enabling detection of both truncated and misfolded HER2—with multiplex editing designed to address and overcome obstacles to maximize efficacy in solid tumor indications. The iPSC-derived, HER2-directed CAR T cells maintained potent HER2-specific anti-tumor activity in both *in vitro* and *in vivo* settings, with limited cytolytic targeting of HER2+ normal targets. Combination with therapeutic antibodies enabled comprehensive multi-antigen targeting through both the CAR and a high-affinity, non-cleavable CD16a Fc receptor. Additionally, specific engineering of interleukin (IL)-7R-fusion, transforming growth factor β (TGF- β)-IL-18R, and CXCR2 enabled sustained persistence, resistance to TGF- β -mediated suppression, and specific migration to the tumor.

INTRODUCTION

Although effective in several hematologic settings, chimeric antigen receptor (CAR) T cells have had limited success in solid tumors. Obstacles to solid tumor efficacy include (1) the challenges in differentiating tumor-associated (TAA) expression between normal and tumor tissue, (2) the heterogeneity of TAA expression within the tumor itself, and (3) absence of successful strategies to simultaneously improve effector cell trafficking to, persistence within, and resistance to the suppression found within the tumor microenvironment (TME).^{1,2}

Human epidermal growth factor receptor 2 (HER2) is overexpressed in multiple solid tumor indications, including breast, gastric, lung, ovarian, and other cancer types.³ Therapeutic targeting of HER2 with antibodies such as trastuzumab (Herceptin) and pertuzumab (Perjeta), or antibody drug conjugates including ado-trastuzumab emtansine (Kadcyla) and fam-trastuzumab deruxtecan-nxki (Enhertu), has shown clinical utility in some pa-

tients.³ Nevertheless, cardiac and pulmonary toxicities may emerge with trastuzumab and trastuzumab-derived therapies, a consequence of HER2 expression in multiple normal tissues, including respiratory epithelia and cardiovascular systems.⁴ Initial efforts with a trastuzumab-based HER2-directed CAR T cell resulted in fatal respiratory failure.⁵ Finally, intrinsic and acquired resistance mechanisms to trastuzumab-based therapies, which have been associated with treatment failure (reviewed in Luque-Cabal et al.⁶ and Ascione et al.⁷), highlight the need for alternative strategies to overcome escape mechanisms and differentially target HER2 in tumor and normal tissue.

Antigen heterogeneity and antigen escape have limited the durability and wider application of CAR T cell therapies. In B cell leukemias and lymphomas, where B cell lineage markers are readily, uniformly, and highly expressed, antigen escape is a major determinant of tumor relapse.^{8–10} TAA expression in solid tumors is substantially more heterogeneous,¹¹ and antigen downregulation and tumor escape have been reported with CAR

T cell treatments targeting a single TAA.¹² Treatment failure with HER2-directed therapies has also been associated with the downregulation and modulation of HER2 expression following trastuzumab,¹³ ado-trastuzumab emtansine,¹⁴ and fam-trastuzumab-deruxtecan-nxki,¹⁵ and constitutively active C-terminal fragments of HER2 (collectively termed p95) that limit trastuzumab effectiveness in preclinical and clinical settings¹⁶ have been observed in up to 30% of all HER2-expressing metastatic breast cancer patients, correlating with disease progression.^{17,18} Clinical benefit has been observed with dual or multi-CAR strategies for B cell lineage antigens that readily overlap in target expression,^{8,19} and, preclinically, dual targeting of multiple solid tumor antigens with either dual CAR or CAR T cell secreting engagers is effective in mitigating antigen escape.^{20,21} Alternatively, CD16a (FcγRIIIa), which is a Fc receptor typically expressed by natural killer (NK) cells, mediates antibody-dependent cell cytotoxicity of opsonized target cells. Expression of a high-affinity²² and non-cleavable variant²³ of CD16a (hnCD16) by induced pluripotent stem cell (iPSC)-derived CAR T and CAR NK cells enables potent and flexible secondary TAA targeting driven by therapeutic antibody administration.²⁴

CD8+ T cell accumulation within solid tumors, along with the expression of pro-inflammatory chemokines such as CXCL9, CXCL10, and CCL5 that support and guide protective anti-tumor responses, is closely correlated with improved clinical outcomes across indications.^{25–28} Alternatively, the misalignment of the chemokines present in the TME and chemokine receptor expression on CD8+ T cells contributes to their inefficient trafficking to solid tumors while also promoting angiogenesis, tumor metastasis, and directing the infiltration of suppressive lymphoid or myeloid immune cell subsets (reviewed in Liu et al.²⁹ and Ozga et al.³⁰). Inefficient effector cell trafficking can be corrected by chemokine receptor engineering to better align CAR T cells with the chemokine milieu present in the TME (reviewed in Foeng et al.³¹). Preclinically, the introduction of CXCR2, whose ligands are enriched in a diverse set of solid tumors and strongly associate with disease burden, enhances intratumoral CAR or TCR-engineered T cell accumulation, improving tumor control.^{32,33}

CAR T cell persistence is correlated with long-term remissions and improved clinical outcomes³⁴; accordingly, CAR T cells have been engineered to express homeostatic or pro-inflammatory cytokines or their signaling components to intrinsically enhance CAR T cell expansion and persistence (reviewed in Bell and Gottschalk³⁵). Interleukin (IL)-7 is a γ_c cytokine that promotes naive and memory T cell homeostatic proliferation.^{36,37} CAR T cells have been engineered to constitutively secrete IL-7^{38,39} or express a constitutively active IL-7 receptor,⁴⁰ promoting T cell survival and enhanced anti-tumor activity. Additionally, constitutive expression of an IL-7-CD127 fusion receptor has been shown to drive ligand-independent IL-7 signaling and improve cytokine-independent engraftment in NSG mice.⁴¹

The TME is further refractory to sustained immune cell activity, the result of both intrinsic and extrinsic factors that converge to restrict and restrain anti-tumor immune cell responses. Transforming growth factor β (TGF- β), a pleiotropic cytokine, is enriched in many different solid tumor types and shapes disease progression, drives metastasis, and inhibits effector cell responses (reviewed in Massagué⁴²). Interference of TGF- β signaling within CAR T cells, either by TGF- β R2 deletion or the

expression of a dominant negative version of TGF- β R2 (dnTGF- β R2), sustains *in vitro* and *in vivo* anti-tumor responses in preclinical modeling.^{43,44} Systemic therapies targeting TGF- β or components of the TGF- β signaling cascade have been advanced to clinical trials for solid tumors, and although they have been generally well tolerated, they have yielded limited clinical benefit to date (reviewed in Kim et al.⁴⁵).

An effective cell therapy for solid tumors will likely need to simultaneously address many of the above obstacles. This is further complicated by available editing tools for autologous or primary allogeneic T cells that are limited by uniformity of the edits, transgene size, safety concerns such as DNA breaks resulting in chromosome translocations,^{46,47} clinical product yield, consistency, and homogeneity of the final drug product (reviewed in Dimitri et al.⁴⁸). The use of iPSCs offers an alternative approach to create off-the-shelf products that are uniformly engineered.^{24,49} Here, we report on the generation and characterization of a HER2-specific, 7-edited iPSC-derived CAR T cell (H2-7E iT, also known as FT825/ONO-8250) that has been precisely engineered to (1) preferentially and potently recognize HER2 expressed by tumor and not normal cells via a HER2-directed CAR in preclinical settings, (2) flexibly target secondary TAAs with hnCD16-mediated antibody-dependent cellular cytotoxicity (ADCC), (3) resist TGF- β -mediated suppression by expression of a TGF- β R2-IL-18R fusion receptor, (4) specifically migrate to CXCR2 ligands as a result of CXCR2 expression, and (5) persist and maintain metabolic activity via expression of an IL-7-IL-7R fusion (IL-7RF) in order to deliver a uniform drug product at scale and enable broad and on-demand patient access.

RESULTS

H₂CasMab-2 recognizes misfolded and truncated variants of HER2

H₂CasMab-2 (also known as H₂Mab-250) is a HER2-specific antibody that selectively binds to HER2 expressed by tumor cells, recognizing a membrane-proximal epitope in domain IV of HER2 between amino acids 613–617 (Figure 1A).⁵⁰ Accordingly, H₂CasMab-2 is capable of binding to both the full length and the p95 C-terminal fragment of HER2. Trastuzumab (clone 4D5), with a more distal and discontinuous recognition epitope between amino acids 579 and 625, is unable to recognize p95 HER2 (Figures 1A–1C). To further characterize the tumor specificity of H₂CasMab-2, we performed a structural analysis of H₂CasMab-2 variable region⁵¹ complexed with amino acids 611–618 of HER2 (Figure S1A). All eight peptide residues were assigned into the electron density observed at the groove between the V_H and V_L domains of H₂CasMab-2. Trp614 occupied a central position in the binding pocket, forming van der Waals contacts with surrounding residues and a hydrogen bond with Ser35 of V_H (Figure S1B), underscoring our previous report demonstrating that Trp614 was critical to HER2 recognition by H₂CasMab-2.⁵⁰ Conventionally, in its native state, this region of HER2 assumes an extended conformation, forming part of a β sheet^{52,53} 22.8 Å in length (Figures 1D and 1F). Instead, when bound by H₂CasMab-2, amino acids 611–618 adopt a bent conformation 15.5 Å in total length, with little resemblance to the native conformation (Figures 1E and 1F). On average, each alpha carbon differed in position from the native conformation

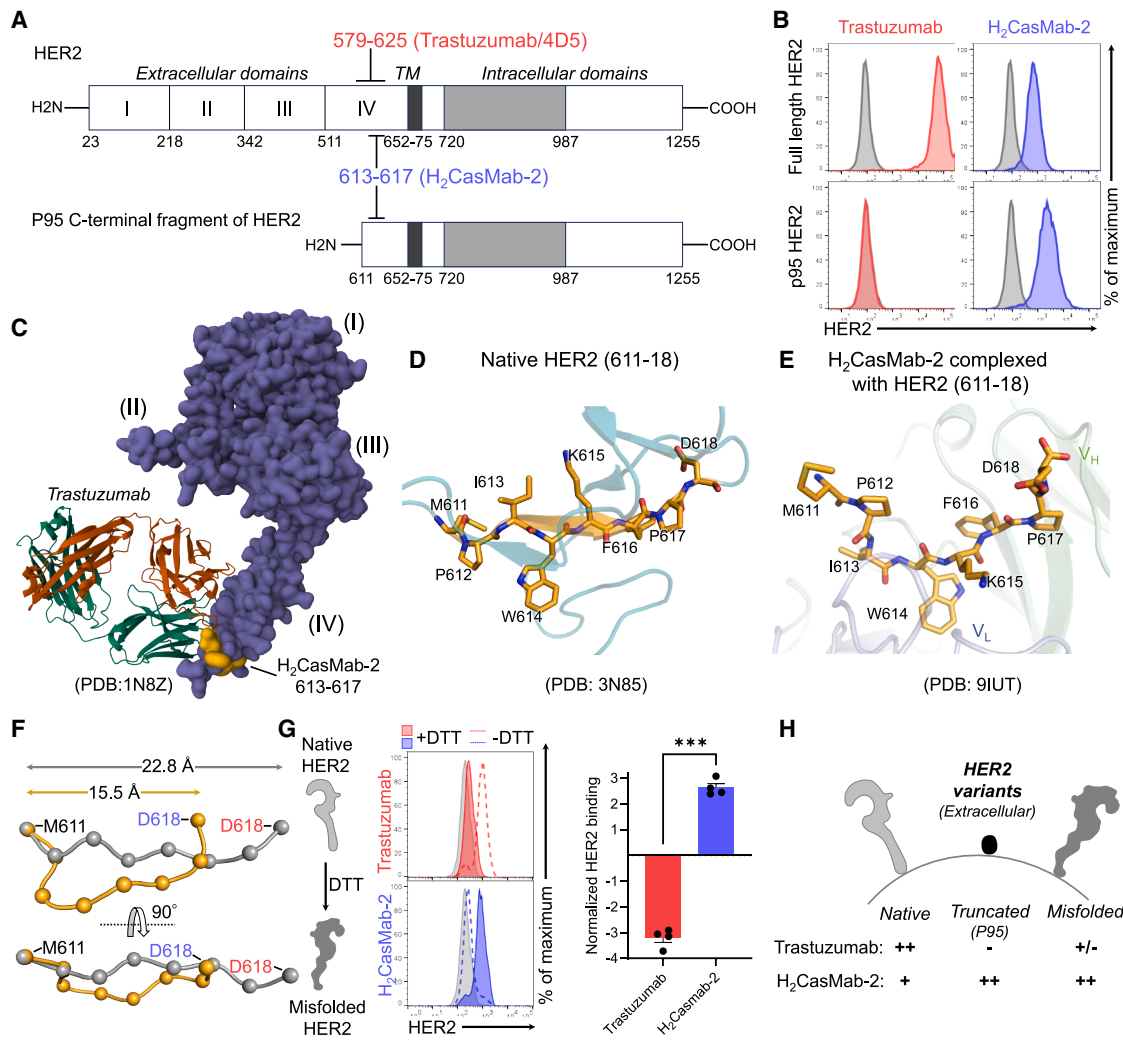


Figure 1. H₂CasMab-2 recognizes misfolded and truncated variants of HER2

(A) Overview of wild-type (WT)/full-length and p95 truncation variants of HER2 with trastuzumab and H₂CasMab-2 binding sites identified. (B) Trastuzumab and H₂CasMab-2 binding to Chinese hamster ovary (CHO) cells engineered to express full-length and p95 human HER2 was evaluated by flow cytometry. (C) Surface projection of the extracellular domains of HER2 (blue) in complex with trastuzumab (PDB: 1N8Z). H₂CasMab-2 binding site is shown in orange. (D and E) Comparison of HER2 611–618 in native HER2 (D, PDB: 3N85) and when bound by H₂CasMab-2 (E, PDB: 9IUT). (F) Overlay of native and H₂CasMab-2-bound HER2 611–618. (G) Endogenous HER2 expression on HEK293T was evaluated by flow cytometry with trastuzumab and H₂CasMab-2 following DTT (filled histograms) or control (dashed lines) treatment. Representative flow cytometry histograms are shown; unstained cells are shown in gray. Normalized HER2 detection relative to the control (no DTT treatment) was quantified; Results are displayed as mean ± SEM; each datapoint represents an independent experiment. ****p* = 0.0002, paired t test. (H) Summary of differential HER2 variant recognition by trastuzumab and H₂CasMab-2.

by ~3 Å, and, as a result, this bent conformation is likely to induce local disruption to neighboring β sheets in domain IV (Figures S1C–S1E).

Preferential binding to misfolded HER2 by other binders that react to similar epitopes as H₂CasMab-2 has been previously observed.⁵⁴ We therefore determined whether H₂CasMab-2 and trastuzumab differentially recognize misfolded compared with native HER2. Normal, non-tumorigenic HEK293T cells that express low, endogenous levels of HER2 were treated with DTT to disrupt protein folding, and HER2 binding by either trastuzumab or H₂CasMab-2 was assessed by flow cytometry. On

control-cultured HEK293T cells, HER2 was readily detected by trastuzumab (red dashed line) compared with H₂CasMab-2 (blue dashed line). DTT pre-treatment significantly reduced (−3.21×, *p* < 0.001) trastuzumab-based detection of HER2 (Figure 1G, red filled histogram). HER2 recognition by H₂CasMab-2, on the other hand, was significantly enhanced (+2.63×, *p* < 0.001) following DTT exposure (Figure 1G, blue filled histogram). These data demonstrate that H₂CasMab-2, compared with trastuzumab, differentially recognizes both locally misfolded HER2 and p95 truncation variants of HER2 in addition to full-length HER2 (Figure 1H).

Differential targeting of tumor rather than normal HER2-expressing cells via H₂CasMab-2 CAR

Given the binding properties and cancer selectivity of H₂CasMab-2,⁵⁰ we generated CAR T cells utilizing trastuzumab (clone 4D5) or H₂CasMab-2 binders in a 2nd generation CD28-based CAR design with a mutated immunoreceptor tyrosine-based activation motif (ITAM) CD3 ζ signaling domain⁵⁵ and evaluated their respective HER2-directed cytotoxicity on a series of HER2^{High} tumor and HER2⁺ normal target lines via xCELLigence real-time cell assay (RTCA) (Figure 2A). HER2 expression of each target tumor or normal cell line, as detected by flow cytometry with a trastuzumab biosimilar, is shown in Figures 2B and 2E, demonstrating high expression of HER2 upon the SKBR3, BT474 (clone 5), OE19, and SKOV3 tumor cells and positive expression of HER2, above unstained or isotype-stained cells, upon MCF10A, MeT-5A, BEAS-2B, THLE2, SV-HUC1, and HTR-8/SVneo normal/non-tumorigenic cells. HER2 staining on a subset of HER2⁺ normal target lines with H₂CasMab-2 revealed no specific staining above unstained controls (Figure S2). Although differences in binding affinity for trastuzumab and H₂CasMab-2 were previously observed on HER2^{High} tumor targets,⁵⁶ both trastuzumab and H₂CasMab-2-based CAR T cells demonstrated similar and potent control of HER2^{High} breast, esophageal, and ovarian tumor targets (Figures 2C and 2F). Conversely, the HER2-directed cytolytic activity of H₂CasMab-2-based CAR T cells was significantly ($p < 0.0001$) reduced on HER2⁺ normal/non-tumorigenic cell lines MCF10A, MeT-5A, BEAS-2B, THLE2, SV-HUC1, and HTR-8/SVneo compared with trastuzumab-based CAR T cells (Figures 2D and 2G). These data demonstrate that, unlike trastuzumab-based CAR T cells, H₂CasMab-2-based CAR T cells differentially and preferentially recognize and lyse HER2^{High} tumor rather than HER2⁺ normal target cells.

Generation and phenotypic characterization of H2-7E iT

Although H₂CasMab-2-based CAR T cells appear to show preferential cancer-specific targeting capacity, effective control of solid tumors by adoptive cell therapy will likely require additional attributes beyond distinguishing TAA expression between tumor and normal tissue.² These additional attributes include (1) overcoming TAA heterogeneity, (2) improving effector cell persistence, (3) enhancing trafficking to the tumor, (4) enabling resistance to the suppressive TME, and (5) preventing T cell exhaustion. It is challenging to develop a cell therapy that consists of multiple engineered attributes using primary T cells.⁴⁸ An iPSC platform presents an attractive solution as it allows for precise multi-gene editing, single-clone selection, and homogeneous effector cell production.²⁴ To overcome the listed challenges in solid tumor therapy, H₂CasMab-2-based CAR and an IL-7-IL-7R α fusion protein (IL-7RF) and TGF- β R2-IL-18R fusion, hnCD16, and CXCR2 were knocked into the T cell receptor, alpha (TRAC), and CD38 loci, respectively, of a single-cell-derived clonal iPSC line (Figure 3A). Engineered iPSCs maintained normal morphology (Figure S3A) and continued to express high and uniform levels of the pluripotency markers SSEA-4, TRA1-81, CD30, OCT4, and NANOG (Figure 3B). Genomic stability of the engineered iPSCs was also confirmed via karyotype (Figure S3B). iPSC-derived CAR T (CAR iT) cells were generated in a stage-specific differentiation protocol^{49,57}

from the clonal multiplex-engineered iPSC line, producing H2-7E iT (Figure 3C). Fully differentiated H2-7E iT cells demonstrated (1) lymphoid commitment (CD45+CD7+); (2) absence of surface TCR $\alpha\beta$ or CD38, the result of transgene engineering into the TRAC or CD38 loci (Figure 3D); and (3) high and homogeneous expression of H₂CasMab-2 CAR, TGF- β R2-IL-18R, hnCD16, and CXCR2 (Figures 3E and S3C).

Preferential and robust targeting of tumor rather than normal HER2 by H2-7E iT

We evaluated the HER2-directed cytotoxicity of H₂CasMab-2 CAR-expressing H2-7E iT on tumor targets with varying levels of HER2 expression (Figure 4A). When co-cultured with HER2-expressing SKOV3 targets, H2-7E iT readily lysed tumor target cells, reaching an EC₅₀ of 1.3:1 (E:T) in a luciferase-based cytolytic assay. Limited cytotoxicity was observed upon HER2^{-/-} targets (Figure 4B), as expected, underscoring the specificity of H2-7E iT via the H₂CasMab-2 CAR for HER2. Next, we evaluated the cytolytic efficacy of H2-7E iT in response to HER2^{High} (3+) SKOV3, HER2⁺ (2+) JIMT1, and HER2^{Low} (0) PC3 tumor target cells. Immunohistochemistry (IHC) scoring and representative flow cytometry for HER2 expression (clone 4D5) on each target line are shown in Figure 4C. Antigen-dependent cytolytic activity, as evaluated by xCELLigence RTCA, was observed by H2-7E iT across each tumor target, from HER2^{High} (3+) to HER2^{Low} (0, Figure 4D). We also evaluated the targeting of HER2⁺ normal cell lines MCF10A and MeT-5A by H2-7E iT and trastuzumab-based primary CAR T cells (Figure 4E). Trastuzumab-based primary CAR T cells readily lysed both MCF10A and MeT-5A target cells. H2-7E iT, on the other hand, demonstrated significantly less ($p < 0.0001$) cytolytic activity on either HER2⁺ normal cell line (Figure 4F), replicating our previous observations with H₂CasMab-2 and trastuzumab-based primary CAR T cells (Figure 2D) and underscoring the HER2 selectivity of H2-7E iT.

The anti-tumor efficacy of H2-7E iT was also evaluated *in vivo* in two separate NSG xenograft models that mirror solid tumor mass engraftment and growth: HER2^{High} (3+) NCI-N87⁵⁸ and HER2^{Low} PC3. NSG mice were challenged with 5×10^5 NCI-N87 subcutaneously (s.c.) and treated intravenously (i.v.) with H2-7E iT starting on day 5 (Figure 4G). H2-7E iT readily controlled the NCI-N87 tumor, maintaining significant tumor control for up to 63 days post effector administration (mean tumor burden 68 days post tumor challenge: 50.2 mm³) compared with vehicle-treated mice (mean tumor burden: 1,167.8 mm³; $p < 0.0001$; Figure 4H). In separate experiments, NSG mice were also challenged with 2×10^6 PC3 s.c. and administered H2-7E iT on day 5 (Figure 4I). Even though PC3 tumor cells express low levels of HER2 (HER2 0+), H2-7E iT still maintained significant but intermediate tumor control (mean tumor burden day 40: 551 mm³) compared with vehicle-treated mice (mean tumor burden: 1,304 mm³, $p < 0.001$, Figure 4J). Importantly, administration of H2-7E iT cells into tumor-bearing or tumor-naive mice did not manifest acute or chronic signs of toxicity, as visualized through similar body weight gains in both settings, no adverse clinical observations, and unremarkable multi-tissue histopathological analysis (Figure S4; data not shown). These data demonstrate that H2-7E iT, as a single agent, demonstrates robust and tumor-preferential HER2-targeted efficacy in both *in vitro* and *in vivo* settings.

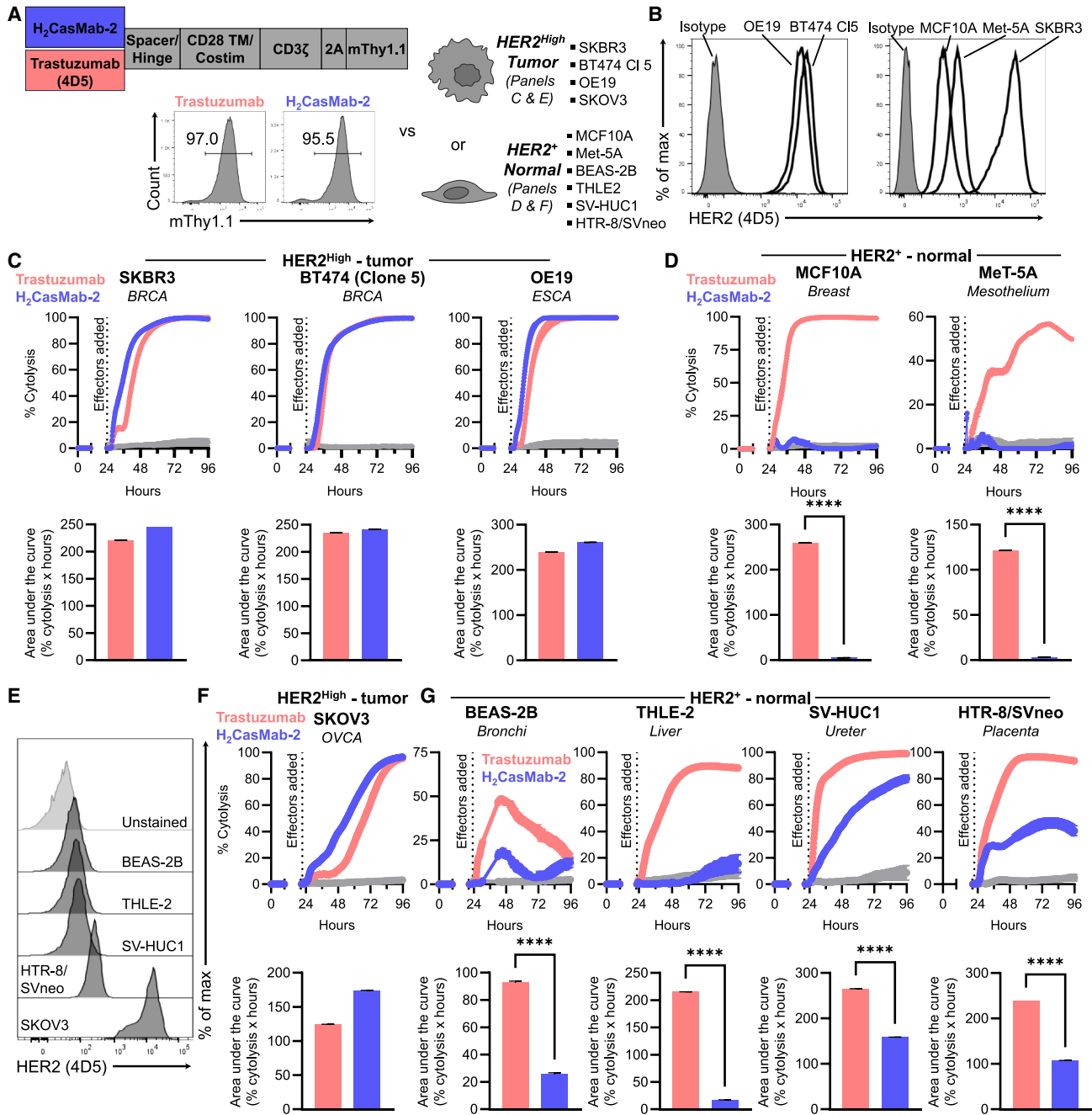


Figure 2. Differential targeting of tumor rather than normal HER2-expressing cells via H₂CasMab-2 CAR

(A) HER2-based cell cytotoxicity (1:1) E:T of primary CAR T cells expressing either trastuzumab (4D5, red) or H₂CasMab-2-based (blue) CARs was evaluated on HER2^{High} tumor (C and F) and HER2⁺ normal (D and G) cell targets. An overview of each HER2 CAR construct is shown, along with representative flow cytometry for banked trastuzumab and H₂CasMab-2-based primary CAR T cells.

(B and E) HER2 expression on the indicated normal and tumor-derived cell lines was determined by flow cytometry.

(C and F) Cytotoxicity on the indicated HER2^{High} tumor cell lines.

(D and G) Cytotoxicity on the indicated HER2⁺ normal cell lines.

Results shown in (C), (D), (F), and (G) are representative of 2–4 independent PBMC donors and displayed as mean ± SEM. Target alone control cultures are shown in gray. Area under the curve analyses are displayed beneath each respective cytotoxicity trace. Significance was determined by unpaired, two-tailed t test; **** $p < 0.0001$. Individual cell line and indication or tissue derivation are noted.

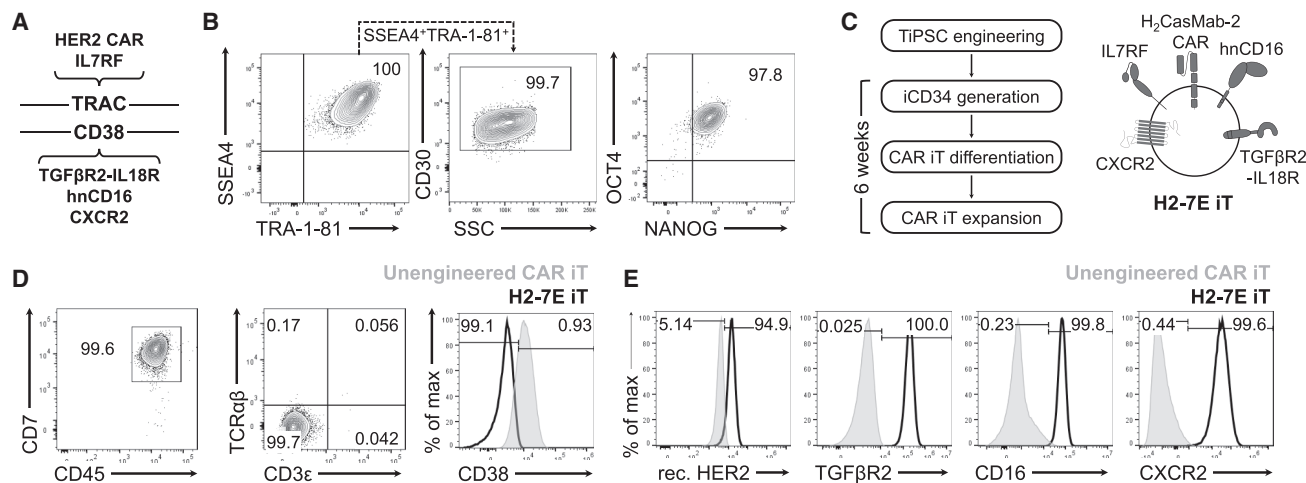


Figure 3. Generation and phenotypic characterization of H2-7E iT

(A) The iPSC multiplex engineering strategy for H2-7E iT.

(B) Representative expression of the pluripotency markers TRA-1-81, SSEA-4, CD30, OCT4, and NANOG as determined by flow cytometry, from fully engineered, T cell-derived iPSCs.

(C) T cell differentiation from TiPSC to a fully differentiated and expanded CAR iT cell: H2-7E iT.

(D and E) Flow cytometry, representative of 3 independent batches of fully differentiated H2-7E iT, shows lymphocyte commitment (CD45+CD7+), no surface TCR $\alpha\beta$ or CD38 expression (D), and high and homogeneous expression of engineered transgenes: H₂CasMab-2 (HER2) CAR, TGF- β R2-IL-18R, hnCD16, and CXCR2 (E). Fully differentiated, unengineered iT cells are shown in gray on the respective histograms.

hnCD16 enables potent and flexible multi-antigen targeting by H2-7E iT

TAA heterogeneity is a significant impediment to CAR T cell function in solid tumors; however, introducing an additional CAR for secondary antigen targeting may increase immune-mediated toxicity.⁵⁹ To enable a multi-antigen strategy that can be temporally controlled and offer flexibility in targeting various antigens in a universal manner, we evaluated whether Fc receptor, namely hnCD16, can enable and support multi-antigen targeting on both HER2^{High} or HER2^{Low} tumor targets with therapeutic antibodies targeting (1) a separate epitope of HER2 with trastuzumab or (2) epidermal growth factor receptor (EGFR) with cetuximab at low E:T ratios. H2-7E iT cells constitutively expressing high levels of hnCD16 (Figures 3E and S3C) were combined with monoclonal antibodies and monitored for cytolytic activity by xCELLigence RTCA (Figure 5A). We utilized HER2^{High} SKOV3 and HER2^{Low} PC3 tumor target cells, which both readily expressed EGFR, as detected by flow cytometry (Figure 5B). At low E:T ratios, H2-7E iT demonstrated intermediate targeting of SKOV3 target cells (blue, Figure 5C). The inclusion of either anti-HER2 (green, top) or anti-EGFR (green, bottom) significantly enhanced the anti-tumor efficacy of H2-7E iT compared with H2-7E iT alone (Figure 5C). Additionally, hnCD16-mediated ADCC was not inhibited by non-specific polyclonal human immunoglobulin G1 (IgG1) (Figures S5A and S5B), underscoring the ability and preference of hnCD16/CD16a to recognize opsonized targets rather than monomeric antibodies.^{60,61} Importantly, the enhanced efficacy observed when anti-HER2 or anti-EGFR antibodies were combined with H2-7E iT was the result of specific hnCD16 activation of ADCC, as no enhanced cytolytic activity was observed in the absence of hnCD16 expression (Figure 5D). CAR expression for H2-7E iT and hnCD16^{neg} HER2 CAR iT cells is shown in Figure S5C. Significantly

improved ($p < 0.0001$) anti-tumor activity was also observed with the inclusion of EGFR-targeting antibodies alongside H2-7E iT and HER2^{Low} PC3 co-cultures (Figure 5E), demonstrating that ADCC via hnCD16 can support multi-antigen targeting on both HER2^{High} and HER2^{Low} target cell lines.

Next, we compared the *in vivo* efficacy of primary HER2 CAR T cells with H2-7E iT, with and without *in vivo* ADCC activation. NSG mice were challenged with 2×10^6 SKOV3 cells s.c., and 8 days later recipient mice were treated separately with either (1) primary H₂CasMab-2 CAR T cells generated from three healthy, independent peripheral mononuclear blood cell (PBMC) donors, (2) trastuzumab, (3) H2-7E iT, or (4) H2-7E iT and trastuzumab. Tumor burden was monitored for 40 days following tumor challenge (Figure 5F). All treatment regimens significantly ($p < 0.0001$) delayed tumor growth compared with vehicle-treated mice (Figure 5G). The anti-tumor efficacy exerted by healthy donor primary HER2 CAR T cells was variable, with final tumor burdens ranging on average from 44 mm³ for donor 3- and 219 mm³ for donor 1-derived cells. H2-7E iT as a monotherapy reduced tumors by approximately 50% and showed comparable activity to trastuzumab-treated mice (mean day 40 tumor burden: 244 versus 189 mm³, $p = 0.0681$) and primary CAR T cell donor (donor 1, $p = 0.8130$, Figure 5H). The combination of H2-7E iT and trastuzumab led to the rapid, complete, and sustained clearance of tumors in all evaluated mice (8/8) that was significantly enhanced relative to H2-7E iT alone, trastuzumab alone, and primary CAR T cell donors 1 and 2 ($p < 0.0001$, Figure 5H). Notably, tumor clearance was only observed in mice receiving the combination of H2-7E iT and trastuzumab. Similar results were seen in similar SKOV3 experiments where the combination of H2-7E iT and trastuzumab led to complete tumor control (5/5 mice) that was significantly enhanced compared with single-agent treatment with either trastuzumab ($p < 0.0001$),

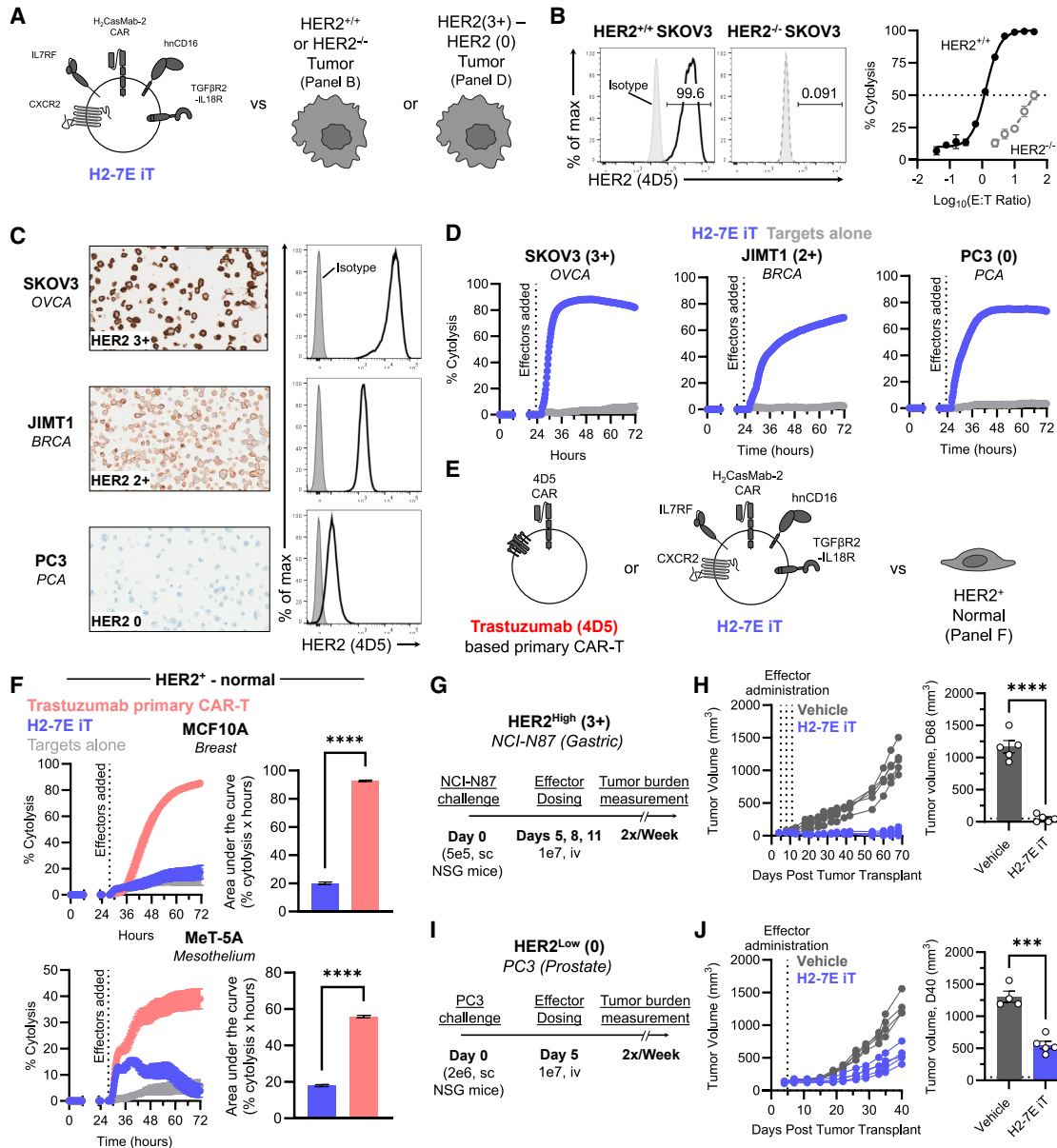


Figure 4. Preferential and robust targeting of tumor rather than normal HER2 by H2-7E iT

(A) Experimental outline for evaluating HER2-mediated targeting of tumor and normal cell lines by H2-7E iT.

(B) HER2 expression of HER2^{+/+} and HER2^{-/-} SKOV3 was determined by flow cytometry. The cytolytic activity of H2-7E iT ($n = 3$) was evaluated on HER2^{+/+} and HER2^{-/-} SKOV3 targets.

(C) HER2 expression of SKOV3, JIMT1, and PC3 tumor cells was evaluated by HER2 IHC (pathway anti-HER2, 4B5, 20 \times magnification; scale bar, 200 μ m) and flow cytometry. HER2 scoring was performed by an independent pathologist.

(D) The cytolytic activity of H2-7E iT against HER2-expressing tumor cells SKOV3, JIMT1, and PC3 (4:1) E:T was determined via xCELLigence RTCA.

(E and F) Experimental outline for comparing the cytolytic efficacy of primary trastuzumab (4D5)-based CAR T and H2-7E iT on HER2⁺ normal cell lines (E). Area under the curve analyses are shown beside each respective cytotoxicity trace (F).

(G–J) The anti-tumor *in vivo* efficacy of H2-7E iT was evaluated in NSG xenograft models with (G) HER2^{High} NCI-N87 or (I) HER2^{Low} PC3. Tumor growth and final tumor burden at the end of each experiment are shown in (H) and (J), respectively. Each dot represents an individual mouse. Exogenous cytokine support was provided in (G).

Data in (D) and (F) are representative of three separate batches of H2-7E iT. Results in (F), (H), and (J) are shown as mean \pm SEM, and significance was determined by unpaired, two-tailed Student's *t* test where **** $p < 0.0001$ and *** $p < 0.001$.

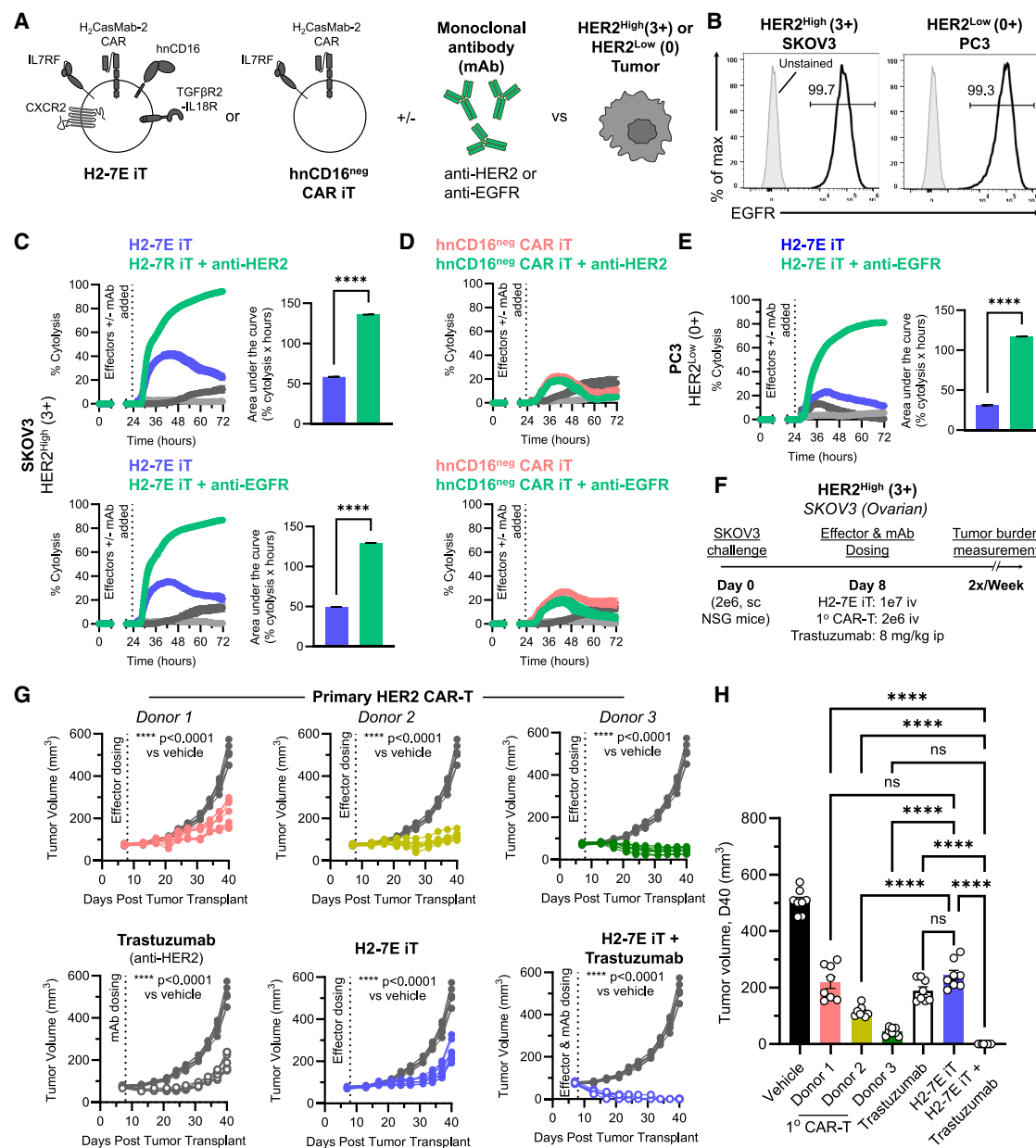


Figure 5. hnCD16 enables potent and flexible multi-antigen targeting by H2-7E iT

(A) Experimental design to evaluate *in vitro* ADCC activation of H2-7E iT compared with hnCD16^{neg} CAR iT cells (TRAC: HER2 CAR/IL-7RF) with HER2^{High} and HER2^{Low} target cells.

(B–E) EGFR expression, as determined by flow cytometry, on HER2^{High} SKOV3 and HER2^{Low} PC3 cells (B). The anti-tumor efficacy of (C) H2-7E iT or (D) hnCD16^{neg} CAR iT cells with or without anti-HER2 or anti-EGFR antibody was evaluated versus HER2^{High} SKOV3 target cells (1:1) E:T via xCELLigence RTCA. The anti-tumor efficacy of H2-7E iT with or without anti-EGFR antibody against HER2^{Low} PC3 target cells (1:1) E:T (E). The dark and light gray lines represent target alone cultures with and without anti-HER2 or anti-EGFR antibody, respectively.

(F) The *in vivo* efficacy of primary CAR T ($n = 3$ donors) and H2-7E iT with or without trastuzumab was evaluated in an NSG xenograft model with s.c. SKOV3 tumor cells.

(G and H) Tumor growth (G) was monitored via caliper measurement, and final tumor burden (H) is shown.

Data in (C)–(E) and (H) are mean \pm SEM, and each symbol in (G) and (H) represents an individual mouse. Significance in (C) and (E) was evaluated by unpaired Student's *t* test and in (G) and (H) by one-way ANOVA with Tukey correction for multiple comparison where *****p* or adjusted *p* < 0.0001.

H2-7E iT ($p < 0.0001$), the antibody drug conjugate fam-trastuzumab-deruxtecan-nxki ($p = 0.0005$), or the combination of hnCD16^{neg} HER2 CAR iT cells with trastuzumab ($p = 0.0113$, Figures S5D–S5F). These data demonstrate that multi-antigen

targeting via H₂CasMab-2 CAR and hnCD16-mediated ADCC by H2-7E iT leads to potent and flexible enhancements in anti-tumor efficacy on HER2^{High} and HER2^{Low} tumor targets in both *in vitro* and *in vivo* settings.

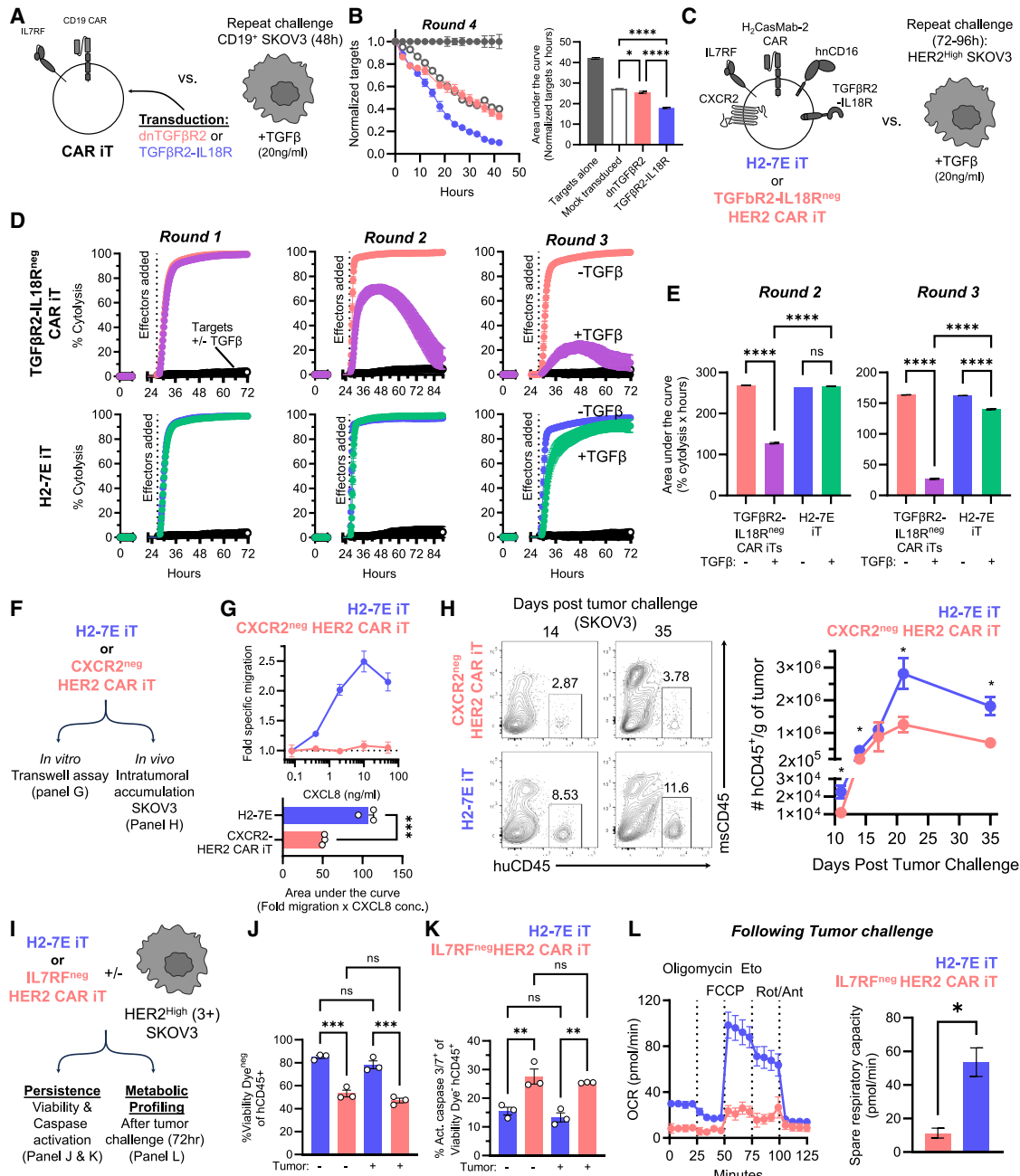


Figure 6. Functional evaluation of TGF-βR2-IL-18R, CXCR2, and IL-7RF in H2-7E iT

(A) dnTGF-βR2 or TGF-βR2-IL-18R were introduced into CAR iT cells and TGF-β resistance was evaluated via repeat tumor challenge in the presence of TGF-β at (2.5:1) E:T.

(B) Round 4 cytolysis and area under the curve analysis are shown comparing mock-transduced (open circles), dnTGF-βR2 (red circles), and TGF-βR2-IL-18R-expressing CAR iT cells (blue circles).

(C) H2-7E iT or TGF-βR2-IL-18R^{neg} HER2 CAR iT cells (TRAC: HER2 CAR/IL-7RF) were repeatedly challenged with HER2^{High} SKOV3 tumor cells ± TGF-β.

(D) Cytotoxicity traces at (2.5:1) E:T for TGF-βR2-IL-18R^{neg} HER2 CAR iT (top row, red and purple) and H2-7E iT (bottom row, blue and green) with (purple and green) or without (red and blue) TGF-β for each round of SKOV3 challenge is shown.

(E) Area under the curve analyses were calculated for rounds two and three.

(F) *In vitro* and *in vivo* evaluation of CXCR2-mediated trafficking by H2-7E iT and CXCR2^{neg} HER2 CAR iT cells (TRAC: HER2 CAR/IL-7RF).

(G) An *in vitro* transwell migration assay with recombinant CXCL8 (IL-8) was performed with H2-7E iT and CXCR2^{neg} HER2 CAR iTs. Fold-specific migration, normalized to baseline chemotaxis, and area under the curve analysis are shown.

(H) SKOV3 tumors from mice previously receiving H2-7E iT or CXCR2^{neg} HER2 CAR iTs were removed and intratumoral CAR iTs were enumerated via flow cytometry at the indicated days post tumor challenge. Representative flow plots and the kinetics of CAR iT accumulation are shown.

(legend continued on next page)

Functional evaluation of TGF- β 2-IL-18R, CXCR2, and IL-7RF in H2-7E iT

We evaluated whether the additional transgenes engineered into H2-7E iT: TGF- β 2-IL-18R, CXCR2, and IL-7RF can enable (1) resistance to TGF- β -mediated suppression, (2) migration to CXCR2 ligands, and (3) enhance their persistence and metabolic functionality, respectively. We first compared the performance of dnTGF- β 2, another common solution for TGF- β resistance,⁴⁴ or TGF- β 2-IL-18R in a short-term (48 h) repeat tumor challenge system in the presence of TGF- β via Incucyte assay (Figure 6A). CAR iT cells transduced to express TGF- β 2-IL-18R maintained significantly ($p < 0.0001$) greater anti-tumor activity compared with mock-transduced or dnTGF- β 2-expressing CAR iT cells after four rounds of tumor challenge in the presence of TGF- β (Figure 6B). Next, we evaluated the ability of H2-7E iT or TGF- β 2-IL-18R^{neg} HER2 CAR iT cells (Figure S6A) to similarly resist repeat challenges in an extended round (72–96 h) repeat challenge model with HER2^{high} SKOV3 tumor targets and TGF- β , via xCELLigence RTCA (Figure 6C). In the absence of TGF- β , both TGF- β 2-IL-18R^{neg} HER2 CAR iT cells (red, top) and H2-7E iT (blue, bottom) maintained high levels of cytotoxicity over three rounds of tumor challenge (Figure 6D). TGF- β inclusion in the assay significantly ($p < 0.0001$) limited the cytolytic activity of HER2 CAR iT cells lacking TGF- β 2-IL-18R expression (purple, top) in rounds 2 and 3 (Figure 6E). H2-7E iT, on the other hand, maintained high levels of anti-tumor efficacy over each round of tumor challenge in the presence of TGF- β (green, bottom, Figure 6D) that was 2–6 \times greater ($p < 0.0001$) than similarly treated TGF- β 2-IL-18R^{neg} HER2 CAR iT cells (Figure 6E). These data demonstrate that the TGF- β 2-IL-18R enables potent and sustained resistance to TGF- β -mediated suppression of effector activity.

Next, we evaluated CXCR2-mediated trafficking of H2-7E iT or CXCR2^{neg} HER2 CAR iT cells in an *in vitro* transwell assay and then separately determined the kinetics of CAR iT accumulation *in vivo* within SKOV3 xenografts (Figure 6F). H2-7E iT or CXCR2^{neg} HER2 CAR iT cells were challenged in a transwell chemotaxis assay with serial dilutions of recombinant human CXCL8 (50 ng/mL–80 pg/mL) and migrated cells were enumerated after 3 h, normalized to their baseline migration in the absence of chemokine. Fold-specific migration and area under the curve analysis are shown in Figure 6G, demonstrating specific and dose-dependent migration of only H2-7E iT in response to multiple concentrations of CXCL8. Next, H2-7E iT and CXCR2^{neg} HER2 CAR iT cells (Figure S6B) were administered to NSG mice previously challenged with SKOV3 tumor cells (Figure S5D). SKOV3 tumors were excised and intratumoral CAR iT cells were quantified (huCD45+msCD45–) by flow cytometry at the indicated days post tumor challenge. Representative flow plots and the overall kinetics of CAR iT accumulation are shown in Figure 6H. SKOV3 cells,⁶² like many solid tumors,⁶³ overexpress CXCR2 ligands.

Accordingly, the intratumoral accumulation of CXCR2-expressing H2-7E iT within SKOV3 xenografts was significantly greater ($p = 0.0243$) than CXCR2^{neg} HER2 CAR iT cells throughout the course of tumor challenge. These data demonstrate that CXCR2 expression by H2-7E iT enables specific migration to CXCR2 ligands and this correlates with enhanced intratumoral accumulation in mouse xenograft models.

Finally, we assessed the role of IL-7RF in sustaining the efficacy of H2-7E iT. We first assessed the expression of phosphorylated STAT5 by H2-7E iT and IL-7RF^{neg} HER2 CAR iT cells (Figure S6C) at rest and in the absence of any exogenous cytokine stimulation and after IL-7 stimulation (Figure S6D). In the absence of γ_c cytokine stimulation (e.g., IL-2, IL-7, and IL-15), H2-7E iT expressed more pSTAT5 relative to IL-7RF^{neg} HER2 CAR iT cells, indicating that IL-7RF expression by H2-7E iT was supporting sustained STAT5 phosphorylation (Figure S6E). Importantly, both IL-7RF^{neg} HER2 CAR iT and H2-7E iT cells remained similarly sensitive to IL-7, rapidly increasing STAT5 phosphorylation within 20 min of stimulation (Figure S6E) and demonstrating that expression of IL-7RF by H2-7E iT does not disrupt endogenous γ_c cytokine signaling. Because IL-7 promotes T cell homeostasis and survival,³⁶ we next evaluated the persistence of H2-7E iT and IL-7RF^{neg} HER2 CAR iT cells after 72 h of (1) neglect or (2) CAR activation in the absence of exogenous cytokine support (Figure 6I). Cell viability was evaluated with viability dye exclusion and flow cytometry. In both stimulation and neglect conditions, a significantly ($p < 0.001$) greater proportion of H2-7E iT cells remained viable (viability dye^{neg}) at the conclusion of the assay compared with IL-7RF^{neg} HER2 CAR iT cells (Figure 6J). Continual IL-7 signaling has been correlated with elevated T cell apoptosis⁶⁴; therefore, we evaluated the expression of activated caspase-3 and -7 by H2-7E iT and IL-7RF^{neg} HER2 CAR iT cells at the end of the assay. As shown in Figure 6K, the frequency of apoptotic cells with or without tumor challenge was significantly reduced ($p < 0.01$) in H2-7E iT compared with IL-7RF^{neg} HER2 CAR iT cells. Transgenic expression of IL-7 has been correlated with sustained metabolic activity of CAR T cells after activation⁶⁵; we therefore measured the mitochondrial respiration of H2-7E iT or IL-7RF^{neg} HER2 CAR iT cells following tumor challenge via Seahorse assay. As shown in Figure 6L, H2-7E iT demonstrated (1) higher overall metabolic activity at baseline and (2) significantly ($p < 0.05$) greater spare respiratory capacity compared with IL-7RF^{neg} HER2 CAR iT cells. Interestingly, (3) the majority (>70%) of metabolic activity measured following FCCP treatment of H2-7E iT was from endogenous fatty acid stores as etomoxir (Eto) had little effect on overall oxygen consumption rate. These data demonstrate that IL-7RF mediates sustained STAT5 phosphorylation within H2-7E iT, and this correlates with enhanced persistence and sustained metabolic activity of H2-7E iT following tumor challenge.

(I–K) Persistence and metabolic profiling evaluation of IL-7RF comparing H2-7E iT and IL-7RF^{neg} HER2 CAR iT cells (TRAC: HER2 CAR, I) after 72 h of neglect (J) or tumor challenge (K).

(L) Metabolic profiling of H2-7E iT and IL-7RF^{neg} CAR iT cells analyzing overall oxygen consumption and spare respiratory capacity.

Results are presented as mean \pm SEM in (B), (E), (G), (H), (J), (K), and (L); symbols represent individual replicates. Significance in (B), (E), (J), and (K) was determined by one-way ANOVA with Tukey correction. Significance in (H) was determined by multiple unpaired t tests with false discovery rate (Benjamini, Krieger, and Yekutieli); and significance in (G) and (L) was determined by unpaired Students t test. **** p or adjusted $p < 0.0001$, *** p or adjusted $p < 0.001$, ** p or adjusted $p < 0.01$, * p , adjusted p , or $q < 0.05$.

DISCUSSION

In this study, we describe H2-7E iT (also known as FT825/ONO-8250), an allogeneic iPSC-derived CAR T cell therapy that combines a HER2-directed CAR that preferentially targets tumor-expressed HER2 and multiplex engineering to enable multi-antigen targeting, enhanced solid tumor trafficking, improved cell persistence, and resistance to TGF- β -mediated suppression. HER2-directed therapies, and, in particular, therapies derived from trastuzumab (Herceptin, Kadcyca, and Enhertu), although effective in treating HER2-positive cancers, have significant pulmonary and cardiac toxicities⁶⁶ due to widespread HER2 expression in normal epithelia.⁴ Moreover, early efforts with primary CAR T cells utilizing a trastuzumab-based CAR resulted in fatal respiratory failure.⁵ Here, we have characterized H₂CasMab-2,^{56,67} a HER2 binder (Figure 1) that recognizes (1) full-length HER2 on HER2-overexpressing tumor cells; (2) p95 HER2, a carboxy truncation of HER2 that correlates with poor clinical outcomes in HER2+ patients^{68,69} and a possible resistance mechanism to trastuzumab-based therapies¹⁶; and (3) locally misfolded HER2, which may be enriched within the TME as a result of a dysfunctional unfolded protein response (reviewed in Oakes⁷⁰). Primary and iPSC-derived CAR T cells utilizing the H₂CasMab-2 binder exhibited robust *in vitro* and *in vivo* HER2-directed cytotoxicity toward both HER2^{high} (3+) and HER2^{Low} (0) tumor target lines. Importantly, both primary and iPSC-derived H₂CasMab-2 CAR T cells produced consistently lower levels of cytotoxicity across a battery of targets from diverse non-tumorigenic tissue sources compared with trastuzumab-based primary CAR T cells (Figures 2 and 4), supporting the hypothesis that HER2-targeted cytolytic activity mediated by the H₂CasMab-2-based CAR of H2-7E iT may preferentially target tumor rather than normal tissue.

In addition to the challenges in limiting the on-target, off-tumor targeting of normal tissue, effective cell therapies for solid tumors have been further limited by antigen heterogeneity and antigen escape, where single-antigen targeting via CAR T cells can lead to a loss of antigen expression within solid tumor settings.^{12,71} Here, we have demonstrated that expression of a high-affinity and non-cleavable version of CD16a^{22,23} by H2-7E iT enables specific, potent, and flexible ADCC, an effector mechanism more commonly associated with NK cells. We have previously demonstrated that iPSC-derived CAR NK or CAR T cells can specifically activate through hnCD16 to enhance anti-tumor targeting and mitigate antigen escape,²⁴ and a recent report with iPSC-derived CAR NK cells underscored their clinical safety.⁷² Utilizing antibodies targeting either EGFR or a separate epitope of HER2, we show in both *in vitro* and *in vivo* settings that hnCD16 co-activation with CAR enhances the anti-tumor efficacy of H2-7E iT (Figures 5 and S5). hnCD16-specific activation of H2-7E iT occurred independent of CAR antigen density of the target, demonstrating that hnCD16 and CAR, though they both activate via CD3 ζ in iPSC-derived CAR T cells, are compatible with and independent of each other. Other solid tumor TAAs that could be targeted in combination with H2-7E iT and FDA-approved, ADCC-enabled therapeutic antibodies, including PD-L1 (avelumab), GD2 (dinutuximab), and VEGFR2 (ramucirumab), can improve outcomes in challenging disease settings.

In addition to the challenges of differentiating between normal and tumor tissue and the heterogeneity of antigen expression within the tumor itself, the TME limits effective immune-mediated anti-tumor responses, a consequence of inefficient effector cell trafficking, direct and indirect immune cell suppression, and limited effector persistence. A defining feature of solid tumors with poor prognoses is often limited effector cell infiltration and their associated inflammatory signature, due, in part, to a mismatch between the chemokines produced within a tumor and the receptor repertoire on immune cell subsets critical for tumor control.^{25–28} CXCR2 ligands are enriched in solid tumors from diverse indications, associating with poor clinical outcomes.²⁹ CXCR2 expression by H2-7E iT enabled specific *in vitro* migration toward CXCL8 and increased their intratumoral accumulation within CXCL8-expressing SKOV3⁶² tumor xenografts (Figure 6). A recent report highlighted the dynamics of CD8+ T cell accumulation within solid tumors, demonstrating a role for endothelial derived CXCL12, a ligand for CXCR4, in promoting lymphatic egress and peripheral localization.⁷³ We hypothesize that constitutive expression of CXCR2 by H2-7E iT may offset the CXCL12-CXCR4-directed exit, improving intratumoral CAR T cell accumulation and retention. TGF- β and its associated signaling signature are widely detected across tumor indications, promoting immune cell suppression and treatment resistance.^{74,75} As a result of TGF- β R2-IL-18R engineering, H2-7E iT resisted the suppressive effects of TGF- β , maintaining effective tumor control over multiple rounds of tumor challenge and TGF- β exposure *in vitro* (Figure 6). Limited clinical efficacy to date has been observed with systemic interference of TGF- β and TGF- β -signaling,⁴⁵ underscoring the need for specific and targeted engineered approaches to subvert TGF- β -mediated effector suppression. Finally, CAR T cell persistence has been correlated with long-term efficacy in liquid tumors³⁴ and is considered a key determinant in solid tumor efficacy. We have engineered H2-7E iT to express IL-7RF, a fusion between IL-7 and IL-7R α that promotes STAT5 phosphorylation in the absence of exogenous ligand (Figure S6). As expected, IL-7RF expression mediated enhanced persistence of H2-7E iT in both conditions of cytokine and antigen withdrawal (neglect) and CAR activation, similar to previous reports.^{37,40,41} Additionally, H2-7E iT maintained enhanced metabolic activity following CAR activation compared with HER2 CAR iT cells (Figure 6), due, in part, to sustained IL-7 signaling via IL-7RF.⁶⁵

As an off-the-shelf, iPSC-derived CAR T cell, engineered to simultaneously address and mitigate many of the primary barriers to CAR T cell therapies for solid tumors, H2-7E iT has been designed to provide significant advantages over similarly targeted autologous or primary allogeneic CAR T cells, including (1) the ability to precisely engineer complex and multiplexed effector strategies, (2) single clonal selection of an iPSC master line that is capable of representing a clonal starting cell source to generate consistent and uniform CAR T cells, and (3) scaled manufacturing to enable off-the-shelf and on-demand patient treatment.⁷⁶

In summary, we have characterized H2-7E iT, an investigational iPSC-derived CAR T cell therapy that combines a HER2-specific binder that preferentially targets tumor-derived HER2 along with

engineered strategies to flexibly enable multi-antigen targeting, avoid TGF- β -mediated effector suppression, improve solid tumor trafficking, and enhance effector persistence. H2-7E iT is currently under investigation in a clinical trial to evaluate safety, pharmacology, and evidence of anti-tumor activity in patients with advanced HER2+ and other solid tumors ([Clinicaltrials.gov NCT06241456](https://clinicaltrials.gov/NCT06241456)).

Limitations of the study

There are limitations to the data presented in this manuscript. First, to compare the HER2 reactivity of trastuzumab and H₂CasMab-2-based primary and iPSC-derived CAR T cells, we have relied upon well-characterized and immortalized cell lines derived from tumor ($n = 4$) or normal tissue ($n = 6$), and although each cell line is expected to be only an approximate representation of its source, we have observed consistent and differential HER2 binding and tumor-selective activity by H₂CasMab-2-based primary and iPSC-derived CAR T cells across these evaluated tumor indications and tissue sources. Second, to illustrate the functionality of specific transgenes engineered into H2-7E iT cells, we have relied upon *in vitro* or *in vivo* xenograft models that are unable to completely capture and replicate the full complexity, heterogeneity, and diversity of patient solid tumors. Ultimately, the translation and application of these preclinical observations, which we hypothesize will enhance the safety and efficacy of H2-7E iT cells, into a clinically relevant and diverse HER2-expressing solid tumor patient population remains to be investigated.

RESOURCE AVAILABILITY

Lead contact

Further information and requests for resources and reagents should be directed to, and will be fulfilled by, the lead contact, Martin P. Hosking (martin.hosking@fatetherapeutics.com).

Materials availability

Novel reagents generated in this study will be made available on request but may require a payment and/or a completed materials transfer agreement if there is potential for commercial application.

Data and code availability

- All data reported in this paper will be shared by the [lead contact](#) upon request, unless restricted by intellectual property rights. Structural analysis of H₂CasMab-2 Fv-clasp complexed with HER2 (611–618) is accessible via PDB: 9iut.
- This paper does not report original code.
- Any additional information required for re-analysis of data will be provided by the [lead contact](#) unless restricted by intellectual property rights.

ACKNOWLEDGMENTS

We would like to acknowledge Howard Fingert, Ono Pharma USA, Inc., and Yu Cai, Fate Therapeutics, Inc., for their critical review and reading of this manuscript. This work was supported in part by JSPS KAKENHI grant number JP21H02416 to T.A.; by Japan Agency for Medical Research and Development (AMED) grant numbers 24am0521010 to Y.K., JP23am0401013 to Y. K., JP23bm1123027 to Y.K., and JP23ck0106730 to Y.K.; and by the Research Support Project for Life Science and Drug Discovery (Basis for Supporting Innovative Drug Discovery and Life Science Research [BINDS]) from AMED under grant numbers JP23ama121011 to J.T. and JP23ama121008 to Y.K.

AUTHOR CONTRIBUTIONS

Conceptualization, M.P.H., S.Y., D.N., E.P., Y.K., and B.V.; methodology and investigation, M.P.H., S.S., K.O., S.C., M.K.K., A.G., B.S., J. Grant, M.B., D. C., H.K., S.I., C.P., T. Mizoguchi, T.I., and T.A.; visualization, M.P.H. and T.A.; funding acquisition, T.A., J.T., and Y.K.; supervision, M.P.H., S.Y., R.A., T.T. L., R.C., J. Goodridge, E.P., J.T., T. Maeda, Y.K., and B.V.; writing – original draft, M.P.H., K.O., S.Y., T. Maeda, T.A., and B.V.; writing – review and editing, M.P.H., K.O., S.C., S.Y., S.I., T. Mizoguchi, T.I., D.N., T. Maeda, T.A., Y. K., and B.V.

DECLARATION OF INTERESTS

M.P.H., S.S., K.O., S.C., A.G., B.S., J. Grant, M.B., D.C., H.K., S.I., C.P., R.A., T.T.L., R.C., J. Goodridge, E.P., and B.V. are employees of Fate Therapeutics Inc. S.Y., T. Mizoguchi, T.I., D.N., and T. Maeda are employees of Ono Pharmaceutical Co., Ltd. Y.K. has received research funding from Ono Pharmaceutical Co., Ltd. Patent applications related to this work have been filed.

STAR★METHODS

Detailed methods are provided in the online version of this paper and include the following:

- [KEY RESOURCES TABLE](#)
- [EXPERIMENTAL MODEL AND STUDY PARTICIPANT DETAILS](#)
 - Animals
 - Cell line culture and reagents
 - Effector assays
 - Luminescence Cytotoxicity analysis
 - xCELLigence RTCA analysis
 - Incucyte Live cell analysis
 - TIPSIC engineering, characterization, and differentiation of iPSC-derived CAR-T cells
- [METHOD DETAILS](#)
 - Flow cytometry
 - H₂CasMab-2 and HER2 peptide crystallization
 - Chemotaxis assay
 - Neglect and activation assay
 - Metabolic profiling
- [QUANTIFICATION AND STATISTICAL ANALYSIS](#)

SUPPLEMENTAL INFORMATION

Supplemental information can be found online at <https://doi.org/10.1016/j.stem.2025.05.007>.

Received: October 14, 2024

Revised: March 24, 2025

Accepted: May 9, 2025

Published: June 4, 2025

REFERENCES

1. Sterner, R.C., and Sterner, R.M. (2021). CAR-T cell therapy: current limitations and potential strategies. *Blood Cancer J.* *11*, 69. <https://doi.org/10.1038/s41408-021-00459-7>.
2. Ramakrishna, S., Barsan, V., and Mackall, C. (2020). Prospects and challenges for use of CAR T cell therapies in solid tumors. *Expert Opin. Biol. Ther.* *20*, 503–516. <https://doi.org/10.1080/14712598.2020.1738378>.
3. Oh, D.-Y., and Bang, Y.-J. (2019). HER2-targeted therapies – a role beyond breast cancer. *Nat. Rev. Clin. Oncol.* *17*, 33–48. <https://doi.org/10.1038/s41571-019-0268-3>.
4. Press, M.F., Cordon-Cardo, C., and Slamon, D.J. (1990). Expression of the HER-2/neu proto-oncogene in normal human adult and fetal tissues. *Oncogene* *5*, 953–962.

- Morgan, R.A., Yang, J.C., Kitano, M., Dudley, M.E., Laurencot, C.M., and Rosenberg, S.A. (2010). Case report of a serious adverse event following the administration of T cells transduced with a chimeric antigen receptor recognizing ERBB2. *Mol. Ther.* *18*, 843–851. <https://doi.org/10.1038/mt.2010.24>.
- Luque-Cabal, M., García-Tejido, P., Fernández-Pérez, Y., Sánchez-Lorenzo, L., and Palacio-Vázquez, I. (2016). Mechanisms behind the Resistance to Trastuzumab in HER2-Amplified Breast Cancer and Strategies to Overcome It. *Clin. Med. Insights Oncol.* *10*, 21–30. <https://doi.org/10.4137/CMO.S34537>.
- Ascione, L., Guidi, L., Prakash, A., Trapani, D., LoRusso, P., Lou, E., and Curigliano, G. (2024). Unlocking the Potential: Biomarkers of Response to Antibody-Drug Conjugates. *Am. Soc. Clin. Oncol. Educ. Book* *44*, e431766. <https://doi.org/10.1200/EDBK.431766>.
- Spiegel, J.Y., Patel, S., Muffly, L., Hossain, N.M., Oak, J., Baird, J.H., Frank, M.J., Shiraz, P., Sahaf, B., Craig, J., et al. (2021). CAR T cells with dual targeting of CD19 and CD22 in adult patients with recurrent or refractory B cell malignancies: a phase 1 trial. *Nat. Med.* *27*, 1419–1431. <https://doi.org/10.1038/s41591-021-01436-0>.
- Majzner, R.G., and Mackall, C.L. (2018). Tumor Antigen Escape from CAR T-cell Therapy. *Cancer Discov.* *8*, 1219–1226. <https://doi.org/10.1158/2159-8290.CD-18-0442>.
- Samur, M.K., Fulciniti, M., Aktas Samur, A.A., Bazarbachi, A.H., Tai, Y.-T., Prabhala, R., Alonso, A., Sperling, A.S., Campbell, T., Petrocca, F., et al. (2021). Biallelic loss of BCMA as a resistance mechanism to CAR T cell therapy in a patient with multiple myeloma. *Nat. Commun.* *12*, 868. <https://doi.org/10.1038/s41467-021-21177-5>.
- Chen, N., Li, X., Chintala, N.K., Tano, Z.E., and Adusumilli, P.S. (2018). Driving CARs on the uneven road of antigen heterogeneity in solid tumors. *Curr. Opin. Immunol.* *51*, 103–110. <https://doi.org/10.1016/j.coi.2018.03.002>.
- O'Rourke, D.M., Nasrallah, M.P., Desai, A., Melenhorst, J.J., Mansfield, K., Morrisette, J.J.D., Martinez-Lage, M., Brem, S., Maloney, E., Shen, A., et al. (2017). A single dose of peripherally infused EGFRvIII-directed CAR T cells mediates antigen loss and induces adaptive resistance in patients with recurrent glioblastoma. *Sci. Transl. Med.* *9*, eaaa0984. <https://doi.org/10.1126/scitranslmed.aaa0984>.
- Mittendorf, E.A., Wu, Y., Scaltriti, M., Meric-Bernstam, F., Hunt, K.K., Dawood, S., Esteva, F.J., Buzdar, A.U., Chen, H., Eksambi, S., et al. (2009). Loss of HER2 Amplification Following Trastuzumab-Based Neoadjuvant Systemic Therapy and Survival Outcomes. *Clin. Cancer Res.* *15*, 7381–7388. <https://doi.org/10.1158/1078-0432.CCR-09-1735>.
- Sakai, H., Tsurutani, J., Iwasa, T., Komoike, Y., Sakai, K., Nishio, K., and Nakagawa, K. (2018). HER2 genomic amplification in circulating tumor DNA and estrogen receptor positivity predict primary resistance to trastuzumab emtansine (T-DM1) in patients with HER2-positive metastatic breast cancer. *Breast Cancer* *25*, 605–613. <https://doi.org/10.1007/s12282-018-0861-9>.
- Mosele, F., Deluche, E., Lusque, A., Le Bescond, L.L., Filleron, T., Pradat, Y., Ducoulombier, A., Pistilli, B., Bachelot, T., Viret, F., et al. (2023). Trastuzumab deruxtecan in metastatic breast cancer with variable HER2 expression: the phase 2 DAISY trial. *Nat. Med.* *29*, 2110–2120. <https://doi.org/10.1038/s41591-023-02478-2>.
- Scaltriti, M., Rojo, F., Ocaña, A., Anido, J., Guzman, M., Cortes, J., Cosimo, S.D., Matias-Guiu, X., Cajal, S.R., Arribas, J., et al. (2007). Expression of p95HER2, a Truncated Form of the HER2 Receptor, and Response to Anti-HER2 Therapies in Breast Cancer. *J. Natl. Cancer Inst.* *99*, 628–638. <https://doi.org/10.1093/jnci/djk134>.
- Sperinde, J., Jin, X., Banerjee, J., Penuel, E., Saha, A., Diedrich, G., Huang, W., Leitzel, K., Weidner, J., Ali, S.M., et al. (2010). Quantitation of p95HER2 in Paraffin Sections by Using a p95-Specific Antibody and Correlation with Outcome in a Cohort of Trastuzumab-Treated Breast Cancer Patients. *Clin. Cancer Res.* *16*, 4226–4235. <https://doi.org/10.1158/1078-0432.CCR-10-0410>.
- Rigakos, G., Razis, E., Koliou, G.-A., Oikonomopoulos, G., Tsolaki, E., Sperinde, J., Chrisafi, S., Zarkavelis, G., Pazarli, E., Batistatou, A., et al. (2021). Evaluation of the Role of p95 HER2 Isoform in Trastuzumab Efficacy in Metastatic Breast Cancer. *Anticancer Res.* *41*, 1793–1802. <https://doi.org/10.21873/anticancer.14945>.
- Shah, N.N., Johnson, B.D., Schneider, D., Zhu, F., Szabo, A., Keever-Taylor, C.A., Krueger, W., Worden, A.A., Kadan, M.J., Yim, S., et al. (2020). Bispecific anti-CD20, anti-CD19 CAR T cells for relapsed B cell malignancies: a phase 1 dose escalation and expansion trial. *Nat. Med.* *26*, 1569–1575. <https://doi.org/10.1038/s41591-020-1081-3>.
- Hirabayashi, K., Du, H., Xu, Y., Shou, P., Zhou, X., Fucá, G., Landoni, E., Sun, C., Chen, Y., Savoldo, B., et al. (2021). Dual-targeting CAR-T cells with optimal costimulation and metabolic fitness enhance antitumor activity and prevent escape in solid tumors. *Nat. Cancer* *2*, 904–918. <https://doi.org/10.1038/s43018-021-00244-2>.
- Choi, B.D., Yu, X., Castano, A.P., Bouffar, A.A., Schmidts, A., Larson, R.C., Bailey, S.R., Boroughs, A.C., Frigault, M.J., Leick, M.B., et al. (2019). CAR-T cells secreting BiTEs circumvent antigen escape without detectable toxicity. *Nat. Biotechnol.* *37*, 1049–1058. <https://doi.org/10.1038/s41587-019-0192-1>.
- Wu, J., Edberg, J.C., Redecha, P.B., Bansal, V., Guyre, P.M., Coleman, K., Salmon, J.E., and Kimberly, R.P. (1997). A novel polymorphism of FcγRIIIa (CD16) alters receptor function and predisposes to autoimmune disease. *J. Clin. Invest.* *100*, 1059–1070. <https://doi.org/10.1172/JCI119616>.
- Jing, Y., Ni, Z., Wu, J., Higgins, L., Markowski, T.W., Kaufman, D.S., and Walcheck, B. (2015). Identification of an ADAM17 Cleavage Region in Human CD16 (FcγRIII) and the Engineering of a Non-Cleavable Version of the Receptor in NK Cells. *PLoS One* *10*, e0121788. <https://doi.org/10.1371/journal.pone.0121788>.
- Cichocki, F., Bjordahl, R., Goodridge, J.P., Mahmood, S., Gaidarova, S., Abujaroud, R., Davis, Z.B., Merino, A., Tuininga, K., Wang, H., et al. (2022). Quadruple gene-engineered natural killer cells enable multi-antigen targeting for durable antitumor activity against multiple myeloma. *Nat. Commun.* *13*, 7341. <https://doi.org/10.1038/s41467-022-35127-2>.
- Ali, H.R., Provenzano, E., Dawson, S.J., Blows, F.M., Liu, B., Shah, M., Earl, H.M., Poole, C.J., Hiller, L., Dunn, J.A., et al. (2014). Association between CD8+ T-cell infiltration and breast cancer survival in 12,439 patients. *Ann. Oncol.* *25*, 1536–1543. <https://doi.org/10.1093/annonc/mdl191>.
- Li, F., Li, C., Cai, X., Xie, Z., Zhou, L., Cheng, B., Zhong, R., Xiong, S., Li, J., Chen, Z., et al. (2021). The association between CD8+ tumor-infiltrating lymphocytes and the clinical outcome of cancer immunotherapy: A systematic review and meta-analysis. *EClinicalMedicine* *41*, 101134. <https://doi.org/10.1016/j.eclinm.2021.101134>.
- Stoll, G., Pol, J., Soumelis, V., Zitvogel, L., and Kroemer, G. (2018). Impact of chemotactic factors and receptors on the cancer immune infiltrate: a bioinformatics study revealing homogeneity and heterogeneity among patient cohorts. *Oncol Immunology* *7*, e1484980. <https://doi.org/10.1080/2162402X.2018.1484980>.
- Dangaj, D., Bruand, M., Grimm, A.J., Ronet, C., Barras, D., Duttagupta, P. A., Lanitis, E., Duraiswamy, J., Tanyi, J.L., Benencia, F., et al. (2019). Cooperation between Constitutive and Inducible Chemokines Enables T Cell Engraftment and Immune Attack in Solid Tumors. *Cancer Cell* *35*, 885–900.e10. <https://doi.org/10.1016/j.ccell.2019.05.004>.
- Liu, Q., Li, A., Tian, Y., Wu, J.D., Liu, Y., Li, T., Chen, Y., Han, X., and Wu, K. (2016). The CXCL8-CXCR1/2 pathways in cancer. *Cytokine Growth Factor Rev.* *31*, 61–71. <https://doi.org/10.1016/j.cytogr.2016.08.002>.
- Ozga, A.J., Chow, M.T., and Luster, A.D. (2021). Chemokines and the immune response to cancer. *Immunity* *54*, 859–874. <https://doi.org/10.1016/j.immuni.2021.01.012>.
- Foeng, J., Comerford, I., and McColl, S.R. (2022). Harnessing the chemokine system to home CAR-T cells into solid tumors. *Cell Rep. Med.* *3*, 100543. <https://doi.org/10.1016/j.xcrm.2022.100543>.

32. Jin, L., Tao, H., Karachi, A., Long, Y., Hou, A.Y., Na, M., Dyson, K.A., Grippin, A.J., Deleyrolle, L.P., Zhang, W., et al. (2019). CXCR1- or CXCR2-modified CAR T cells co-opt IL-8 for maximal antitumor efficacy in solid tumors. *Nat. Commun.* *10*, 4016. <https://doi.org/10.1038/s41467-019-11869-4>.
33. Peng, W., Ye, Y., Rabinovich, B.A., Liu, C., Lou, Y., Zhang, M., Whittington, M., Yang, Y., Overwijk, W.W., Lizée, G., et al. (2010). Transduction of Tumor-Specific T Cells with CXCR2 Chemokine Receptor Improves Migration to Tumor and Antitumor Immune Responses. *Clin. Cancer Res.* *16*, 5458–5468. <https://doi.org/10.1158/1078-0432.CCR-10-0712>.
34. Melenhorst, J.J., Chen, G.M., Wang, M., Porter, D.L., Chen, C., Collins, M. A., Gao, P., Bandyopadhyay, S., Sun, H., Zhao, Z., et al. (2022). Decade-long leukaemia remissions with persistence of CD4+ CAR T cells. *Nature* *602*, 503–509. <https://doi.org/10.1038/s41586-021-04390-6>.
35. Bell, M., and Gottschalk, S. (2021). Engineered Cytokine Signaling to Improve CAR T Cell Effector Function. *Front. Immunol.* *12*, 684642. <https://doi.org/10.3389/fimmu.2021.684642>.
36. Schluns, K.S., Kieper, W.C., Jameson, S.C., and Lefrançois, L. (2000). Interleukin-7 mediates the homeostasis of naïve and memory CD8 T cells in vivo. *Nat. Immunol.* *1*, 426–432. <https://doi.org/10.1038/80868>.
37. Rathmell, J.C., Farkash, E.A., Gao, W., and Thompson, C.B. (2001). IL-7 Enhances the Survival and Maintains the Size of Naive T Cells. *J. Immunol.* *167*, 6869–6876. <https://doi.org/10.4049/jimmunol.167.12.6869>.
38. Perna, S.K., Pagliara, D., Mahendravada, A., Liu, H., Brenner, M.K., Savoldo, B., and Dotti, G. (2014). Interleukin-7 Mediates Selective Expansion of Tumor-redirected Cytotoxic T Lymphocytes (CTLs) without Enhancement of Regulatory T-cell Inhibition. *Clin. Cancer Res.* *20*, 131–139. <https://doi.org/10.1158/1078-0432.CCR-13-1016>.
39. Adachi, K., Kano, Y., Nagai, T., Okuyama, N., Sakoda, Y., and Tamada, K. (2018). IL-7 and CCL19 expression in CAR-T cells improves immune cell infiltration and CAR-T cell survival in the tumor. *Nat. Biotechnol.* *36*, 346–351. <https://doi.org/10.1038/nbt.4086>.
40. Shum, T., Omer, B., Tashiro, H., Kruse, R.L., Wagner, D.L., Parikh, K., Yi, Z., Sauer, T., Liu, D., Parihar, R., et al. (2017). Constitutive Signaling from an Engineered IL7 Receptor Promotes Durable Tumor Elimination by Tumor-Redirected T Cells. *Cancer Discov.* *7*, 1238–1247. <https://doi.org/10.1158/2159-8290.CD-17-0538>.
41. Hunter, M.R., Prosser, M.E., Mahadev, V., Wang, X., Aguilar, B., Brown, C. E., Forman, S.J., and Jensen, M.C. (2013). Chimeric γ c cytokine receptors confer cytokine independent engraftment of human T lymphocytes. *Mol. Immunol.* *56*, 1–11. <https://doi.org/10.1016/j.molimm.2013.03.021>.
42. Massagué, J. (2008). TGF β in Cancer. *Cell* *134*, 215–230. <https://doi.org/10.1016/j.cell.2008.07.001>.
43. Tang, N., Cheng, C., Zhang, X., Qiao, M., Li, N., Mu, W., Wei, X.-F., Han, W., and Wang, H. (2020). TGF- β inhibition via CRISPR promotes the long-term efficacy of CAR-T cells against solid tumors. *JCI Insight* *5*, e133977. <https://doi.org/10.1172/jci.insight.133977>.
44. Kloss, C.C., Lee, J., Zhang, A., Chen, F., Melenhorst, J.J., Lacey, S.F., Maus, M.V., Fraietta, J.A., Zhao, Y., and June, C.H. (2018). Dominant-Negative TGF- β Receptor Enhances PSMA-Targeted Human CAR T Cell Proliferation And Augments Prostate Cancer Eradication. *Mol. Ther.* *26*, 1855–1866. <https://doi.org/10.1016/j.ymthe.2018.05.003>.
45. Kim, B.-G., Malek, E., Choi, S.H., Ignatz-Hoover, J.J., and Driscoll, J.J. (2021). Novel therapies emerging in oncology to target the TGF- β pathway. *J. Hematol. Oncol.* *14*, 55. <https://doi.org/10.1186/s13045-021-01053-x>.
46. Mickelthwaite, K.P., Gowrishankar, K., Gloss, B.S., Li, Z., Street, J.A., Moezzi, L., Mach, M.A., Suttrave, G., Clancy, L.E., Bishop, D.C., et al. (2021). Investigation of product-derived lymphoma following infusion of piggyBac-modified CD19 chimeric antigen receptor T cells. *Blood* *138*, 1391–1405. <https://doi.org/10.1182/blood.2021010858>.
47. Shah, N.N., Qin, H., Yates, B., Su, L., Shalabi, H., Raffeld, M., Ahlman, M. A., Stetler-Stevenson, M., Yuan, C., Guo, S., et al. (2019). Clonal expansion of CAR T cells harboring lentivector integration in the CBL gene following anti-CD22 CAR T-cell therapy. *Blood Adv.* *3*, 2317–2322. <https://doi.org/10.1182/bloodadvances.2019000219>.
48. Dimitri, A., Herbst, F., and Fraietta, J.A. (2022). Engineering the next-generation of CAR T-cells with CRISPR-Cas9 gene editing. *Mol. Cancer* *21*, 78. <https://doi.org/10.1186/s12943-022-01559-z>.
49. van der Stegen, S.J.C., Lindenberg, P.L., Petrovic, R.M., Xie, H., Diop, M. P., Alexeeva, V., Shi, Y., Mansilla-Soto, J., Hamieh, M., Eyquem, J., et al. (2022). Generation of T-cell-receptor-negative CD8 α β -positive CAR T cells from T-cell-derived induced pluripotent stem cells. *Nat. Biomed. Eng.* *6*, 1284–1297. <https://doi.org/10.1038/s41551-022-00915-0>.
50. Kaneko, M.K., Suzuki, H., and Kato, Y. (2024). Establishment of a Novel Cancer-Specific Anti-HER2 Monoclonal Antibody H2Mab-250/H2CasMab-2 for Breast Cancers. *Monoclon. Antib. Immunodiagn. Immunother.* *43*, 35–43. <https://doi.org/10.1089/mab.2023.0033>.
51. Arimori, T., Kitago, Y., Umitsu, M., Fujii, Y., Asaki, R., Tamura-Kawakami, K., and Takagi, J. (2017). Fv-clasp: An Artificially Designed Small Antibody Fragment with Improved Production Compatibility, Stability, and Crystallizability. *Structure* *25*, 1611–1622.e4. <https://doi.org/10.1016/j.str.2017.08.011>.
52. Cho, H.-S., Mason, K., Ramyar, K.X., Stanley, A.M., Gabelli, S.B., Denney, D.W., and Leahy, D.J. (2003). Structure of the extracellular region of HER2 alone and in complex with the Herceptin Fab. *Nature* *421*, 756–760. <https://doi.org/10.1038/nature01392>.
53. Eigenbrot, C., Ultsch, M., Dubnovitsky, A., Abrahmsén, L., and Härd, T. (2010). Structural basis for high-affinity HER2 receptor binding by an engineered protein. *Proc. Natl. Acad. Sci. USA* *107*, 15039–15044. <https://doi.org/10.1073/pnas.1005025107>.
54. Arimori, T., Mihara, E., Suzuki, H., Ohishi, T., Tanaka, T., Kaneko, M.K., Takagi, J., and Kato, Y. (2024). Locally misfolded HER2 expressed on cancer cells is a promising target for development of cancer-specific antibodies. *Structure* *32*, 536–549.e5. <https://doi.org/10.1016/j.str.2024.02.007>.
55. Feucht, J., Sun, J., Eyquem, J., Ho, Y.-J., Zhao, Z., Leibold, J., Dobrin, A., Cabriolu, A., Hamieh, M., and Sadelain, M. (2019). Calibration of CAR activation potential directs alternative T cell fates and therapeutic potency. *Nat. Med.* *25*, 82–88. <https://doi.org/10.1038/s41591-018-0290-5>.
56. Kaneko, M.K., Suzuki, H., Ohishi, T., Nakamura, T., Tanaka, T., and Kato, Y. (2024). A Cancer-Specific Monoclonal Antibody against HER2 Exerts Antitumor Activities in Human Breast Cancer Xenograft Models. *Int. J. Mol. Sci.* *25*, 1941. <https://doi.org/10.3390/ijms25031941>.
57. Valamehr, B., Robinson, M., Abujarour, R., Rezner, B., Vranceanu, F., Le, T., Medcalf, A., Lee, T.T., Fitch, M., Robbins, D., et al. (2014). Platform for Induction and Maintenance of Transgene-free hiPSCs Resembling Ground State Pluripotent Stem Cells. *Stem Cell Rep.* *2*, 366–381. <https://doi.org/10.1016/j.stemcr.2014.01.014>.
58. Bezman, N.A., Kim, C.C., Sun, J.C., Min-Oo, G., Hendricks, D.W., Kamimura, Y., Best, J.A., Goldrath, A.W., and Lanier, L.L.; Immunological Genome Project Consortium (2012). Molecular definition of the identity and activation of natural killer cells. *Nat. Immunol.* *13*, 1000–1009. <https://doi.org/10.1038/ni.2395>.
59. Hegde, M., Corder, A., Chow, K.K.H., Mukherjee, M., Ashoori, A., Kew, Y., Zhang, Y.J., Baskin, D.S., Merchant, F.A., Brawley, V.S., et al. (2013). Combinational Targeting Offsets Antigen Escape and Enhances Effector Functions of Adoptively Transferred T Cells in Glioblastoma. *Mol. Ther.* *21*, 2087–2101. <https://doi.org/10.1038/mt.2013.185>.
60. Li, P., Jiang, N., Nagarajan, S., Wohlhueter, R., Selvaraj, P., and Zhu, C. (2007). Affinity and Kinetic Analysis of Fc γ Receptor IIIa (CD16a) Binding to IgG Ligands*. *J. Biol. Chem.* *282*, 6210–6221. <https://doi.org/10.1074/jbc.M609064200>.
61. Bruhns, P., Iannascoli, B., England, P., Mancardi, D.A., Fernandez, N., Jorieux, S., and Daéron, M. (2009). Specificity and affinity of human Fc γ receptors and their polymorphic variants for human IgG subclasses. *Blood* *113*, 3716–3725. <https://doi.org/10.1182/blood-2008-09-179754>.
62. Gatla, H.R., Zou, Y., Uddin, M.M., Singha, B., Bu, P., Vancura, A., and Vancurova, I. (2017). Histone Deacetylase (HDAC) Inhibition Induces I κ B

- Kinase (IKK)-dependent Interleukin-8/CXCL8 Expression in Ovarian Cancer Cells. *J. Biol. Chem.* 292, 5043–5054. <https://doi.org/10.1074/jbc.M116.771014>.
63. Lazennec, G., Rajarathnam, K., and Richmond, A. (2024). CXCR2 chemokine receptor – a master regulator in cancer and physiology. *Trends Mol. Med.* 30, 37–55. <https://doi.org/10.1016/j.molmed.2023.09.003>.
64. Kimura, M.Y., Pobeziński, L.A., Guinter, T.I., Thomas, J., Adams, A., Park, J.-H., Tai, X., and Singer, A. (2013). IL-7 signaling must be intermittent, not continuous, during CD8⁺ T cell homeostasis to promote cell survival instead of cell death. *Nat. Immunol.* 14, 143–151. <https://doi.org/10.1038/ni.2494>.
65. Li, L., Li, Q., Yan, Z.-X., Sheng, L.-S., Fu, D., Xu, P., Wang, L., and Zhao, W.-L. (2022). Transgenic expression of IL-7 regulates CAR-T cell metabolism and enhances in vivo persistence against tumor cells. *Sci. Rep.* 12, 12506. <https://doi.org/10.1038/s41598-022-16616-2>.
66. Tamura, K., Tsurutani, J., Takahashi, S., Iwata, H., Krop, I.E., Redfern, C., Sagara, Y., Doi, T., Park, H., Murthy, R.K., et al. (2019). Trastuzumab deruxtecan (DS-8201a) in patients with advanced HER2-positive breast cancer previously treated with trastuzumab emtansine: a dose-expansion, phase 1 study. *Lancet Oncol.* 20, 816–826. [https://doi.org/10.1016/s1470-2045\(19\)30097-x](https://doi.org/10.1016/s1470-2045(19)30097-x).
67. Suzuki, H., Ohishi, T., Tanaka, T., Kaneko, M.K., and Kato, Y. (2024). Anti-HER2 Cancer-Specific mAb, H2Mab-250-hG1, Possesses Higher Complement-Dependent Cytotoxicity than Trastuzumab. *Int. J. Mol. Sci.* 25, 8386. <https://doi.org/10.3390/ijms25158386>.
68. Sáez, R., Molina, M.A., Ramsey, E.E., Rojo, F., Keenan, E.J., Albanell, J., Lluch, A., García-Conde, J., Baselga, J., and Clinton, G.M. (2006). p95HER-2 Predicts Worse Outcome in Patients with HER-2-Positive Breast Cancer. *Clin. Cancer Res.* 12, 424–431. <https://doi.org/10.1158/1078-0432.CCR-05-1807>.
69. Chumsri, S., Sperinde, J., Liu, H., Gligorov, J., Spano, J.-P., Antoine, M., Moreno Aspitia, A.M., Tan, W., Winslow, J., Petropoulos, C.J., et al. (2018). High p95HER2/HER2 Ratio Associated With Poor Outcome in Trastuzumab-Treated HER2-Positive Metastatic Breast Cancer NCCTG N0337 and NCCTG 98-32-52 (Alliance). *Clin. Cancer Res.* 24, 3053–3058. <https://doi.org/10.1158/1078-0432.CCR-17-1864>.
70. Oakes, S.A. (2020). Endoplasmic Reticulum Stress Signaling in Cancer Cells. *Am. J. Pathol.* 190, 934–946. <https://doi.org/10.1016/j.ajpath.2020.01.010>.
71. Brown, C.E., Alizadeh, D., Starr, R., Weng, L., Wagner, J.R., Naranjo, A., Ostberg, J.R., Blanchard, M.S., Kilpatrick, J., Simpson, J., et al. (2016). Regression of Glioblastoma after Chimeric Antigen Receptor T-Cell Therapy. *N. Engl. J. Med.* 375, 2561–2569. <https://doi.org/10.1056/NEJMoa1610497>.
72. Ghobadi, A., Bachanova, V., Patel, K., Park, J.H., Flinn, I., Riedell, P.A., Bachier, C., Diefenbach, C.S., Wong, C., Bickers, C., et al. (2025). Induced pluripotent stem-cell-derived CD19-directed chimeric antigen receptor natural killer cells in B-cell lymphoma: a phase 1, first-in-human trial. *Lancet* 405, 127–136. [https://doi.org/10.1016/S0140-6736\(24\)02462-0](https://doi.org/10.1016/S0140-6736(24)02462-0).
73. Steele, M.M., Jaiswal, A., Delclaux, I., Dryg, I.D., Murugan, D., Femel, J., Son, S., du Bois, H., Hill, C., Leachman, S.A., et al. (2023). T cell egress via lymphatic vessels is tuned by antigen encounter and limits tumor control. *Nat. Immunol.* 24, 664–675. <https://doi.org/10.1038/s41590-023-01443-y>.
74. Battle, E., and Massagué, J. (2019). Transforming Growth Factor- β Signaling in Immunity and Cancer. *Immunity* 50, 924–940. <https://doi.org/10.1016/j.immuni.2019.03.024>.
75. Zhang, M., Zhang, Y.Y., Chen, Y., Wang, J., Wang, Q., and Lu, H. (2021). TGF- β Signaling and Resistance to Cancer Therapy. *Front. Cell Dev. Biol.* 9, 786728. <https://doi.org/10.3389/fcell.2021.786728>.
76. Cichocki, F., van der Stegen, S.J.C., and Miller, J.S. (2023). Engineered and banked iPSCs for advanced NK- and T-cell immunotherapies. *Blood* 141, 846–855. <https://doi.org/10.1182/blood.2022016205>.
77. Tomayko, M.M., and Reynolds, C.P. (1989). Determination of subcutaneous tumor size in athymic (nude) mice. *Cancer Chemother. Pharmacol.* 24, 148–154. <https://doi.org/10.1007/BF00300234>.
78. Kabsch, W. (2010). XDS. *Acta Crystallogr. D Biol. Crystallogr.* 66, 125–132. <https://doi.org/10.1107/S0907444909047337>.
79. McCoy, A.J., Grosse-Kunstleve, R.W., Adams, P.D., Winn, M.D., Storoni, L.C., and Read, R.J. (2007). Phaser crystallographic software. *J. Appl. Crystallogr.* 40, 658–674. <https://doi.org/10.1107/S0021889807021206>.
80. Winn, M.D., Ballard, C.C., Cowtan, K.D., Dodson, E.J., Emsley, P., Evans, P.R., Keegan, R.M., Krissinel, E.B., Leslie, A.G.W., McCoy, A., et al. (2011). Overview of the CCP4 suite and current developments. *Acta Crystallogr. D Biol. Crystallogr.* 67, 235–242. <https://doi.org/10.1107/S0907444910045749>.
81. Adams, P.D., Afonine, P.V., Bunkóczi, G., Chen, V.B., Davis, I.W., Echols, N., Headd, J.J., Hung, L.W., Kapral, G.J., Grosse-Kunstleve, R.W., et al. (2010). PHENIX: a comprehensive Python-based system for macromolecular structure solution. *Acta Crystallogr. D Biol. Crystallogr.* 66, 213–221. <https://doi.org/10.1107/S0907444909052925>.
82. Emsley, P., Lohkamp, B., Scott, W.G., and Cowtan, K. (2010). Features and development of Coot. *Acta Crystallogr. D Biol. Crystallogr.* 66, 486–501. <https://doi.org/10.1107/S0907444910007493>.
83. Chen, V.B., Arendall, W.B., Headd, J.J., Keedy, D.A., Immormino, R.M., Kapral, G.J., Murray, L.W., Richardson, J.S., and Richardson, D.C. (2010). MolProbity: all-atom structure validation for macromolecular crystallography. *Acta Crystallogr. D Biol. Crystallogr.* 66, 12–21. <https://doi.org/10.1107/S0907444909042073>.

STAR★METHODS

KEY RESOURCES TABLE

REAGENT or RESOURCE	SOURCE	IDENTIFIER
Antibodies		
Anti-HER2 (H ₂ CasMab-2)	This Paper	N/A
Anti-HER2 (4D5/ <i>trastuzumab</i> biosimilar, conjugated)	R&D Systems	Cat#: FAB9589R; RRID: AB_3654059
Anti-HER2 (4D5/ <i>trastuzumab</i> biosimilar, unconjugated)	R&D Systems	Cat#: MAB9896; RRID: AB_2934014
APC anti-mouse IgG1 (clone RMG1-1)	Biologend	Cat#: 406610; RRID: AB_10696420
Anti-HER2 (<i>trastuzumab</i>)	Roche	NDC: 50242-132-01; RRID: AB_3669039
Anti-EGFR (<i>cetuximab</i>)	MedChemExpress	Cat#: HY-P9905; RRID: AB_3694544
Anti-Thy1.1 (murine, clone OX-7)	BD Biosciences	Cat#: 554898; RRID: AB_395589
Anti-SSEA4 (human, clone MC813-70)	BD Biosciences	Cat#: 560126; RRID: AB_1645491
Anti-TRA-1-81 (human, clone TRA-1-81)	BD Biosciences	Cat#: 560793; RRID: AB_10550550
Anti-CD30 (human, clone BerH8)	BD Biosciences	Cat#: 550041; RRID: AB_393541
Anti-OCT4 (human, clone 40/Oct-3)	BD Biosciences	Cat#: 565644; RRID: AB_2739320
Anti-Nanog (human, clone N31-355)	BD Biosciences	Cat#: 561300; RRID: AB_10611718
Anti-CD7 (human, clone M-T701)	BD Biosciences	Cat#: 564019; RRID: AB_2738545
Anti-CD45 (human, clone HI30)	BD Biosciences	Cat#: 563792; RRID: AB_2869519
Anti-TCR $\alpha\beta$ (human, clone T10B9.1A-31)	BD Biosciences	Cat#: 563825; RRID: AB_2687420
Anti-CD3 (human, clone UCHT1)	Biologend	Cat#: 300452; RRID: AB_2564148
Anti-CD38 (human, clone HB-7)	Biologend	Cat#: 356614; RRID: AB_2562183
Anti-TGF β R2 (human, clone W17055E)	Biologend	Cat#: 399712; RRID: AB_2927906
Anti-CD16 (human, clone 3G8)	BD Biosciences	Cat#: 562874; RRID: AB_2716865
Anti-CXCR2 (human, clone 5E8)	Biologend	Cat#: 320706; RRID: AB_439807
Anti-EGFR (human, clone AY13)	Biologend	Cat#: 352904; RRID: AB_10896794
Anti-STAT5, pY694 (human, Clone 47)	BD Biosciences	Cat#: 562984; RRID: AB_2737931
F(ab') ₂ Fragment Goat Anti-Mouse IgG	Jackson ImmunoResearch	Cat#: 115-606-072; RRID: AB_2338928
Anti-CD45 (murine, clone 30-F11)	Biologend	Cat#: 103147; RRID: AB_2564383
Fixable viability dye	Invitrogen	Cat#: 65-0865-14
Activated Caspase 3/7	Invitrogen	Cat#: C10423
Bacterial and virus strains		
HER2 (4D5) CAR lentivirus	This paper	N/A
HER2 (H ₂ CasMab-2) CAR lentivirus	This paper	N/A
dnTGF β R lentivirus	This paper	N/A
TGF β R2-IL18R lentivirus	This paper	N/A
Biological samples		
Human Peripheral Blood Mononuclear Cells, Fresh	StemCell Technologies	Cat#: 200-0078
Chemicals, peptides, and recombinant proteins		
Recombinant human HER2, biotinylated	Acro Biosystems	Cat#: HE2-H82E2
Streptavidin-PE	BD Biosciences	Cat#: 554061
Recombinant human IL-8/CXCL8	R&D Systems	Cat#: 208-IL/CF
TGF β	R&D Systems	Cat#: 7754-BH/CF
IL-2	Clinigen	NDC: 76310-022-01

(Continued on next page)

Continued

REAGENT or RESOURCE	SOURCE	IDENTIFIER
Critical commercial assays		
xCELLigence Real-Time Cell Analysis MP	Agilent Technologies	N/A
Incucyte S3	Sartorius	RRID: SCR_023147
ONE-Glo Luciferase Assay System	Promega	Cat#: E6110
SpectraMax ID5	Molecular Devices	N/A
XFe96 Extracellular Flux Analyzer	Seahorse	RRID: SCR_019545
Deposited data		
H ₂ CasMab-2 Fv-clasp complexed with HER2 (611-18)	This paper	PDB: 9iut
Experimental models: Cell lines		
SKBR3	ATCC	Cat#: HTB-30; RRID: CVCL_0033
BT474 (Clone 5)	ATCC	Cat#: CRL-3247; RRID: CVCL_AQ07
OE19	Sigma	Cat#: 96071721-1VL; RRID: CVCL_1622
MCF10a	ATCC	Cat#: CRL-10317; RRID: CVCL_0598
Met-5a	Ono Pharmaceuticals	N/A; RRID: CVCL_3749
SKOV3	ATCC	Cat#: HTB-77; RRID: CVCL_0532
BEAS-2B	ATCC	Cat#: CRL-3588; RRID: CVCL_0168
THLE-2	ATCC	Cat#: CRL-2706; RRID: CVCL_3803
SV-HUC1	ATCC	Cat#: CRL-9520; RRID: CVCL_3798
HTR-8/SVneo	ATCC	Cat#: CRL-3271; RRID: CVCL_7162
JIMT1	AddexBio	Cat#: C0006005; RRID: CVCL_2077
NCI-N87	ATCC	Cat#: CRL-5822; RRID: CVCL_1603
PC3	ATCC	Cat#: CRL-1435; RRID: CVCL_0035
Experimental models: Organisms/strains		
Mouse: NOD.Cg-Prkdc ^{scid} Il2rg ^{tm1Wjl} /SzJ (NSG)	The Jackson Laboratory	Cat#: 005557; RRID: IMSR_JAX:005557
Software and algorithms		
FlowJo	BD Biosciences	Version 10.8.1
Prism	GraphPad	Version 10.4.1 (627)
FACSDiva	BD Biosciences	Version 9
CytExpert	Beckman Coulter	Version 2.6
OMIQ	OMIQ	https://www.omiq.ai/
SoftMax Pro	Molecular Devices	Version 7.1.2
Incucyte	Sartorius	Version 2022A
RTCA Software Pro with Immunotherapy module	Agilent	Version 2.3.4.2001

EXPERIMENTAL MODEL AND STUDY PARTICIPANT DETAILS

Animals

6-week-old male or female NSG (NOD.Cg-Prkdc^{scid} Il2rg^{tm1Wjl}/SzJ) were purchased from Jackson Laboratories. And subcutaneously inoculated in the left flank with NCI-N87 (5x10⁵), PC3 (2x10⁶), or SKOV3 (2x10⁶) tumor cells diluted 1:1 in HBSS and Matrigel (NCI-N87, SKOV3) or Cultrex (PC3). HER2 CAR iT (10x10⁶) or primary CAR-T (2x10⁶) cells were administered intravenously and tumor burden was measured 2x weekly via caliper measurement.⁷⁷ Prior to effector, antibody, and/or antibody drug conjugate treatment, mice were randomized based on tumor burden to equalize tumor burden between treatment groups. Trastuzumab (20mg/kg; Herceptin, Roche) and fam-trastuzumab-deruxtecan-nxki (5.4mg/kg; Enhertu, Daiichi Sankyo,) was administered intravenously where indicated. Intratumoral CAR iT cells were evaluated *ex vivo* from excised and digested tumors (gentleMACS, Miltenyi Biotec) by flow cytometry. All studies were approved by the institution's Institutional Animal Care and Use Committee and were conducted in accordance with the National Institutes of Health's Guide for the Care and Use of Laboratory Animals at Fate Therapeutics Torrey Pines campus. Mice were group housed in irradiated caging in one of two 300 square foot rooms maintained between 68°F-76°F and 30-70% humidity. Irradiated or autoclaved enrichment was provided. In addition to oversight by a board-certified laboratory animal

veterinarian, all animal technicians are rigorously trained and certified. Microbiological, clinical pathological, and necropsy diagnostic services are available.

Cell line culture and reagents

The human cell lines SKOV3 (HTB-77), SKBR3 (HTB-30), BT474 Clone 5 (CRL-3247), PC3 (CRL-1435), NCI-N87 (CRL5822), MCF10A (CRL-10317), MeT-5A (CRL-9444), THLE-2 (CRL-2706), SV-HUC-1 (CRL-9520), BEAS-2B (CRL-9609), HEK293T (CRL-3216), and HTR-8/SVneo (CRL-3271) were obtained from ATCC. JIMT1 and OE19 cells were acquired from AddexBio and Millipore Sigma, respectively. HER2 knockout SKOV3 cells were a kind gift from Bruce Walcheck, University of Minnesota. CHO-K1 cells were obtained from *JCRB Cell Bank* (Japanese Collection of Research Bioresources Cell Bank) and engineered to express full length or p95 HER2. All cell lines were cultured according to manufacturer instructions. HER2 immunohistochemistry was performed with overnight fixed (10% neutral buffered formalin) and paraffin-embedded cells. HER2 staining and pathologist scoring were performed at Mosaic Laboratories according to manufacturer guidelines.

Effector assays

Primary CAR Ts were generated from healthy donors following activation with anti-CD3/28 Dynabeads (1:1, ThermoFisher). After 24 hours, cells were spinoculated (650xg, 1hr 32°C) with lentivirus encoding each specific CAR construct and polybrene (4 µg/ml). Dynabeads were removed on day 4 and transduced cells were enriched by Thy1.1 positive selection (Stemcell Technologies) on day 8. CAR transduction efficiency was evaluated by Thy1.1 expression.

Luminescence Cytotoxicity analysis

Target cells engineered to express firefly luciferase were co-cultured with effector cells at serially diluted effector-to-target (E:T) ratios in CTS OpTmizer media (Gibco) in 96-well plates. After overnight incubation, the remaining viable target cells were assessed by measuring the production of luciferase using the ONE-Glo Luciferase Assay System (Promega) and the SpectraMax iD5 plate reader (Molecular Devices). The luminescent signal across different E:T ratios was normalized to target cell only signal and the dose-dependent curve was fitted to a 4-parameter logistic curve to calculate the half-maximal effective concentration (EC50) values using SoftMax Pro software (Molecular Devices).

xCELLigence RTCA analysis

Target cells ($1-4 \times 10^4$) were plated in culture media in a 96 well E-Plate (Agilent Technologies). Approximately 24 hours later, culture media was removed and effector cells in CTS OpTmizer media (Gibco) were added at indicated E:T ratios. For restimulation assays, effector cells were collected at the end of each round, counted and replated on fresh target cells at the indicated E:T ratio. For evaluation of ADCC, 10µg/ml of Herceptin/trastuzumab (Roche) or Erbitux/cetuximab (MedChemExpress) was added with effectors. For functional assessment of TGFβR2-IL18R, media was supplemented with 10ng/ml of TGFβ (R&D Systems). Cytolysis was measured by xCELLigence RTCA MP and RTCA Software Pro with Immunotherapy module (Agilent Technologies). Area under the curve analyses were performed in GraphPad Prism.

Incucyte Live cell analysis

Target cells expressing NucLightGreen (NLG) were seeded in 48-well plates at 2.5×10^4 cells/well and incubated overnight. On the day of effector addition, culture media was removed and effector cells diluted in CTS OpTmizer media (Gibco) were added at indicated E:T ratio with IL-2 (125U/ml; Proimmune). At the end of each round, effector cells were collected, counted and replated on fresh target cells at the indicated E:T ratio. Target cell cytotoxicity was monitored with Incucyte software v2022A using a mask on NLG+ nuclei. Collected data underwent a two-step normalization process prior to visualization. Targets were normalized to the number of NLG+ nuclei at time zero, and then normalized a second time to the number of NLG+ nuclei in the target cell alone negative control well at each time point. Area under the curve analyses were performed in GraphPad Prism.

TiPSC engineering, characterization, and differentiation of iPSC-derived CAR-T cells

H2-7E iT was engineered from T cell-derived induced pluripotent stem cells as previously described.^{49,57} Briefly, H₂CasMab-2 CAR and IL7RF and TGFβ-IL18R, hnCD16, and CXCR2 were CRISPR engineered into TRAC or CD38 loci, respectively, via Neon electroporation (ThermoFisher) according to manufacturer instructions. Following electroporation, individual clones were separated and screened for site specific integration, genomic stability, and preserved pluripotency. Human TiPSC differentiation to iCD34+ cells, differentiation into T cell lineage, and T cell expansion were performed as previously described.⁴⁹

METHOD DETAILS

Flow cytometry

Single cell suspensions were surface stained with fluorophore-conjugated antibodies to human SSEA4, TRA-1-81, CD30, CD7, CD45, TCRαβ, CD3ε, CD38, TGFβR2, CD16, and CXCR2 and murine CD45 (BD Biosciences and BioLegend, San Diego, USA). HER2 expression was evaluated with either a fluorophore-conjugated or unconjugated trastuzumab biosimilar antibody (4D5, R&D Systems) or with unconjugated H₂CasMab-2 antibody. The unconjugated antibodies were secondary stained with fluorophore-conjugated anti-mouse IgG

(BioLegend or Thermo Fisher Scientific). H₂CasMab-2 CAR expression was detected by staining with biotinylated HER2 recombinant protein (Acro Biosystems) then PE-Streptavidin (BD Biosciences) or with directly conjugated goat anti-mouse IgG, F(ab')₂ fragment specific (Jackson ImmunoResearch). For surface staining, cells were incubated for 30 min at 4°C with antibodies/protein diluted in BSA Stain Buffer (BD Biosciences). Intracellular staining with fluorophore-conjugated antibodies to human OCT4 and NANOG (BD Biosciences) was performed using FoxP3 Transcription Factor Staining Buffer Set (eBiosciences). STAT5 phosphorylation was evaluated in effector cells rested overnight in CTS OpTmizer media (Gibco) then incubated 20 min with and without IL7 (15ng/ml; R&D Systems). Cells were fixed and permeabilized with Phosphoflow Perm Buffer III according to manufacturer's instructions (BD Biosciences) and stained with anti-phosphorylated STAT5 (pY694; BD Biosciences). Fluorescently stained cells were collected on SA3800 Cell Analyzer (Sony Corp.), BD Fortessa (BD Biosciences), or CytoFLEX (Beckman Coulter) and analyzed with FlowJo (BD Biosciences) or OMIQ (OMIQ) software.

H₂CasMab-2 and HER2 peptide crystallization

As previously described,⁵¹ the C-terminus of the V_H (1-113) and V_L domains of H₂CasMab-2 were fused to the SARAH domain from human MST1 and the Fc domain of hulgG1 (234-447). Fc-fused H₂CasMab-2 Fv-clasp were expressed and purified from Expi293F cells (Thermo Fisher Scientific). Fc-fused H₂CasMab-2 Fv-clasp were subsequently digested with IdeS protease for 2 hours at 37°C, purified via anion-exchange chromatography, and concentrated by ultrafiltration (Amicon Ultra, Merck Millipore). H₂CasMab-2 Fv-clasp were mixed with 611-618 of HER2 (MPIWKFPD) to a final concentration of 3.5 mg/ml H₂CasMab-2 Fv-clasp and 0.3 mM peptide. Diffraction quality crystals were generated via hanging drop vapor-diffusion with 0.2 M MgCl₂, 0.1 M Bis-Tris pH 5.7, 25 % w/v polyethylene glycol (PEG) 3350, cryoprotected in mother liquor with 30% PEG3350, and flash cooled in liquid nitrogen. Diffraction data were collected at 100 K on beamline BL44XU at SPring-8 (Harima, Japan). The data were indexed, integrated, and scaled using X-ray Detector Software.⁷⁸ Initial phases were determined by molecular replacement method with PHASER⁷⁹ in the CCP4 package⁸⁰ using the coordinates deposited in Protein Data Bank (PDB): PDB: 3liz (V_H), PDB: 3sge (V_L), and PDB: 7cea (SARAH domain). The structural models were refined with PHENIX⁸¹ and COOT⁸² and subsequently validated with MolProbity.⁸³ Data collection statistics and refinement parameters are summarized in Table S1.

Chemotaxis assay

Thawed effector cells were rested overnight in CTS OpTmizer media (Gibco) and then washed twice with RPMI media (Cytiva) supplemented with 0.5% BSA Fraction V (EMD Millipore). CXCL8, serially diluted 1:5 in 0.5% BSA RPMI to achieve a concentration range of 50ng/ml to 0.08ng/ml, was aliquoted in the bottom chamber of 24-well transwell plates and incubated for 10 min. Effector cells (1 × 10⁶) were then plated in the upper chamber of the transwell plates and incubated at 37 °C for 3hrs. Migrated cells were enumerated by FACS using SPHERO counting beads (Spherotech). Data acquisition was performed on a Fortessa instrument (BD LSRFortessa X-20), using FACSDiva software. Analyses were performed using FlowJo v10 (FlowJo LLC, Ashland, OR). Absolute cell numbers within each condition were normalized the no CXCL8 condition to obtain a fold specific migration value.

Neglect and activation assay

Effectors cells (2 × 10⁴ cells) resuspended in CTS OpTmizer media (Gibco) were plated into 96-well plates with/without target cells and incubated at 37°C for 72hrs. For tumor target activation condition, tumor cells were seeded a night before at 2 × 10⁴ cells/well. Cells were collected and stained with fixable viability dye (Invitrogen) and for Caspase-3/7 (Invitrogen) expression according to manufacturer's instructions. Cells were subsequently stained with anti-human CD45 and EpCAM. Data acquisition was performed on a Fortessa instrument (BD LSRFortessa X-20), using FACSDiva software. Analyses were performed using FlowJo v10 (FlowJo LLC, Ashland, OR). Effectors cells were identified as CD45+ and EpCAM-.

Metabolic profiling

Oxygen consumption rate (OCR) was measured in a XFe96 Extracellular Flux Analyzer (Seahorse). Briefly, SKOV3 targets were pre-seeded at 1e5/mL in 6 well plates. One day later, effector cells, diluted in CTS media, were added at 10:1 E:T. and harvested after 48 hours of co-culture for metabolic profiling. Effector cells were resuspended in RPMI XF medium (Agilent,103576), containing 1M Glucose (Agilent, 103577), 1mM sodium pyruvate (Agilent, 103578) and 2mM Glutamine (Thermo Fisher, 25-005-CI) at 1.5e5 per well, into 96-well PDL Plate (Agilent, 103799). OCR was assessed by addition of oligomycin (10μM), carbonyl cyanide-4-(trifluoromethoxy)phenylhydrazine (FCCP, 20μM), etomoxir (100μM), and antimycin A (10μM)/Rotenone (1μM) at the indicated time points. Data were collected on Wave Software (version 2.6.3) and analyzed using GraphPad Prism (version 10.2).

QUANTIFICATION AND STATISTICAL ANALYSIS

Data analysis and visualization was performed using Prism 10.4.1 (GraphPad Software). Graphs represent group mean values ± SEM, as noted in the figure legends. All statistical tests conducted were two-sided, and p<0.05 was considered statistically significant. Significance values were indicated with asterisks: **** = p<0.0001, *** = p<0.001, ** = p<0.01, * = p<0.05, ns = p > 0.05. Statistical tests performed: paired and unpaired t-tests, multiple unpaired t tests with False Discovery Rate (Benjamini, Krieger, and Yekutieli), and one-way ANOVA with Tukey's multiple comparison tests, group sizes, and repeat experiments performed are described in the relevant figure legends.